Tropical teleconnection impacts on Antarctic climate changes

Xichen Li[1]✉, Wenju Cai[2,3,4], Gerald A. Meehl[5], Dake Chen[6,7], Xiaojun Yuan[8], Marilyn Raphael[9], David M. Holland[10,11], Qinghua Ding[12], Ryan L. Fogt[13], Bradley R. Markle[12,14], Guojian Wang[2,3,4], David H. Bromwich[15], John Turner[16], Shang-Ping Xie[17], Eric J. Steig[18], Sarah T. Gille[17], Cunde Xiao[19], Bingyi Wu[20], Matthew A. Lazzara[21,22], Xianyao Chen[2,3], Sharon Stammerjohn[14], Paul R. Holland[16], Marika M. Holland[5], Xiao Cheng[7,23], Stephen F. Price[24], Zhaomin Wang[7,25], Cecilia M. Bitz[26], Jiuxin Shi[27], Edwin P. Gerber[10], Xi Liang[28], Hugues Goosse[29], Changhyun Yoo[30], Minghu Ding[31], Lei Geng[32], Meijiao Xin[1], Chuanjin Li[33], Tingfeng Dou[34], Chengyan Liu[7,25], Weijun Sun[35], Xinyue Wang[1] and Chentao Song[1]

Abstract | Over the modern satellite era, substantial climatic changes have been observed in the Antarctic, including atmospheric and oceanic warming, ice sheet thinning and a general Antarctic-wide expansion of sea ice, followed by a more recent rapid loss. Although these changes, featuring strong zonal asymmetry, are partially influenced by increasing greenhouse gas emissions and stratospheric ozone depletion, tropical–polar teleconnections are believed to have a role through Rossby wave dynamics. In this Review, we synthesize understanding of tropical teleconnections to the Southern Hemisphere extratropics arising from the El Niño–Southern Oscillation, Interdecadal Pacific Oscillation and Atlantic Multidecadal Oscillation, focusing on the mechanisms and long-term climatic impacts. These teleconnections have contributed to observed Antarctic and Southern Ocean changes, including regional rapid surface warming, pre-2015 sea ice expansion and its sudden reduction thereafter, changes in ocean heat content and accelerated thinning of most of the Antarctic ice sheet. However, due to limited observations and inherent model biases, uncertainties remain in understanding and assessing the importance of these teleconnections versus those arising from greenhouse gases, ozone recovery and internal variability. Sustained pan-Antarctic efforts towards long-term observations, and more realistic dynamics and parameterizations in high-resolution climate models, offer opportunities to reduce these uncertainties.

Southern Annular Mode (SAM). The leading mode of extratropical Southern Hemisphere atmospheric circulation, characterized by pressure variability between the mid and high southern latitudes, influencing the strength and position of the mid-latitude jet.

✉e-mail: *lixichen@mail.iap.ac.cn*

https://doi.org/10.1038/s43017-021-00204-5

Over the course of the satellite era, a series of rapid and interconnected climatic changes have been observed over Antarctica and the Southern Ocean. For example, subsurface ocean temperature and ocean heat content increased[1–3], surface air temperatures (SATs) rose over West Antarctica and the Antarctic Peninsula[4,5], many ice shelves and portions of the ice sheet experienced thinning[6,7] and hemispheric sea ice increased up until 2015 but decreased rapidly thereafter[8–12]. These changes have marked implications for polar ecosystems[13,14], sea level rise[15,16], water mass formation and ocean circulation[17–19].

Such shifts have been attributed to several factors. These include changes in the Southern Annular Mode (SAM)[20], particularly a trend towards positive phases associated with increased greenhouse gas (GHG) emissions and stratospheric ozone loss[21–24]. Anthropogenic warming[25] and internal multidecadal variability of the Antarctic–Southern Ocean system[8,26,27] are also thought to have contributed to observed changes. However, none of these factors, including anthropogenic forcings, are able to fully explain the observed surface changes, particularly their seasonality and spatial heterogeneity.

In West Antarctica, for instance, near-surface air temperature increases are twice the global average[4,5,28]. In East Antarctica, by contrast, negligible warming or slight cooling has occurred, with an overall (albeit uncertain) increase in ice mass[29]. Moreover, before the sudden sea ice loss starting in 2015, Antarctic sea ice extent increased amidst anthropogenic warming

Anthropogenic forcings
Climatic forcings linked to anthropogenic factors, typically, increased greenhouse gas concentrations associated with fossil fuel burning, sulfate aerosols produced as an industrial by-product, stratospheric ozone depletion and human-induced changes in land surface properties.

(the so-called sea ice paradox), with a regional redistribution of sea ice between the Ross Sea and Amundsen–Bellingshausen Seas[30–32]. These zonally asymmetric changes cannot be fully explained by anthropogenic forcings[4,5,28,29,33–36]. Instead, variability in the circulation of the Amundsen Sea Low (ASL) — linked to internal tropical ocean variability and subsequent tropical–polar teleconnections — has been found to be important[5,34,36–39].

The notion of a tropical–polar connection has long been established, as demonstrated by the known impact of the El Niño–Southern Oscillation (ENSO) on Antarctica. During El Niño events, convective heating of the tropical atmosphere generates stationary Rossby wave trains[40–47] with alternating centres of high-pressure and low-pressure anomalies, curving poleward and eastward towards Antarctica (and the Arctic; see BOX 1), where they interact with the ASL. Combined with internal variability, driven in particular by the SAM[48] and, possibly, the Antarctic Circumpolar Wave[49], these anomalous circulation features impact interannual sea ice distribution, SAT and precipitation through wind-driven dynamic and thermodynamic responses[50–53].

Following a growing body of evidence suggesting that teleconnections can also originate from other tropical oceans[28,54–58], that their combined impact can be substantial[59] and that they can operate on multidecadal timescales[47], tropical trends and subsequent tropical–polar connections have emerged as an active area of research for understanding longer-term climatic changes in Antarctica. In particular, multidecadal sea surface temperature (SST) variability associated with the Interdecadal Pacific Oscillation (IPO) and the Atlantic Multidecadal Oscillation (AMO) is believed to be a potential driver of multidecadal changes in Antarctica through low-frequency modulation of tropical–polar teleconnections and their time-averaged impact[58].

In this Review, we synthesize progress on tropical–polar teleconnections, focusing on their relationships with multidecadal climatic change in Antarctica. We begin by reviewing the physical mechanisms governing tropical–Antarctic teleconnections on interannual timescales, followed by a discussion of their impacts. Next, we outline how such mechanisms apply on multidecadal timescales and their role in driving contemporary climatic change in Antarctica. We end by considering how teleconnections might change in the future and offer future research priorities.

Interannual teleconnections

Before considering the decadal-scale influence of tropical–polar teleconnections, it is important to first consider their mechanisms on interannual timescales, the impacts of which form the basis of any longer-term effects (FIG. 1). Considering that ENSO events dominate tropical climate variability on interannual timescales[60], driving observed circum-Antarctic climatic changes, ENSO-related teleconnections are used as the foundation for understanding Southern Hemisphere tropical–polar connections. Focus is given to atmospheric circulation anomalies associated with stationary planetary waves and the zonal-mean circulation, before discussing teleconnections emanating from the tropical Atlantic and Indian Ocean.

Stationary wave dynamics

The most widely recognized teleconnection mechanism is a stationary Rossby wave. When generated by an ENSO event, the atmospheric signature of this wave train is referred to as the Pacific–South American (PSA) pattern[61,62] (FIG. 1a). In the case of an El Niño event, the PSA pattern is initially related to positive SST anomalies in the tropical Pacific. Depending on how these SST anomalies project onto background climatological conditions, thresholds of 27.5 °C can be exceeded

Author addresses

[1]Institute of Atmospheric Physics, Chinese Academy of Sciences, Beijing, China.
[2]Frontiers Science Center for Deep Ocean Multispheres and Earth System and Physical Oceanography Laboratory, Ocean University of China, Qingdao, China.
[3]Qingdao National Laboratory for Marine Science and Technology, Qingdao, China.
[4]Centre for Southern Hemisphere Oceans Research (CSHOR), CSIRO Oceans and Atmosphere, Hobart, TAS, Australia.
[5]Climate and Global Dynamics Laboratory, National Center for Atmospheric Research, Boulder, CO, USA.
[6]Second Institute of Oceanography, Ministry of Natural Resources, Hangzhou, China.
[7]Southern Marine Science and Engineering Guangdong Laboratory (Zhuhai), Zhuhai, China.
[8]Lamont-Doherty Earth Observatory, Columbia University, New York, NY, USA.
[9]Department of Geography, University of California, Los Angeles, Los Angeles, CA, USA.
[10]Courant Institute of Mathematical Sciences, New York University, New York, NY, USA.
[11]Center for Global Sea Level Change, New York University Abu Dhabi, Abu Dhabi, UAE.
[12]Department of Geography and Earth Research Institute, University of California, Santa Barbara, Santa Barbara, CA, USA.
[13]Department of Geography, Ohio University, Athens, OH, USA.
[14]Institute of Arctic and Alpine Research, University of Colorado, Boulder, CO, USA.
[15]Byrd Polar & Climate Research Center and Atmospheric Sciences Program, The Ohio State University, Columbus, OH, USA.
[16]British Antarctic Survey, Natural Environment Research Council, Cambridge, UK.
[17]Scripps Institution of Oceanography, University of California, San Diego, La Jolla, CA, USA.
[18]Department of Earth and Space Sciences, University of Washington, Seattle, WA, USA.
[19]State Key Laboratory of Earth Surface Processes and Resource Ecology, Beijing Normal University, Beijing, China.
[20]Department of Atmospheric and Oceanic Sciences and Institute of Atmospheric Sciences, Fudan University, Shanghai, China.
[21]Space Science and Engineering Center, University of Wisconsin–Madison, Madison, WI, USA.
[22]Department of Physical Sciences, Madison Area Technical College, Madison, WI, USA.
[23]School of Geospatial Engineering and Science, Sun Yat-sen University, Zhuhai, China.
[24]Fluid Dynamics and Solid Mechanics Group, Los Alamos National Laboratory, Los Alamos, NM, USA.
[25]College of Oceanography, Hohai University, Nanjing, China.
[26]Department of Atmospheric Sciences, University of Washington, Seattle, WA, USA.
[27]Key Laboratory of Physical Oceanography, Ocean University of China, Qingdao, China.
[28]Key Laboratory of Research on Marine Hazards Forecasting, National Marine Environmental Forecasting Center, Beijing, China.
[29]Earth and Life Institute, Université catholique de Louvain (UCLouvain), Louvain-la-Neuve, Belgium.
[30]Department of Climate and Energy Systems Engineering, Ewha Womans University, Seoul, South Korea.
[31]Institute of Tibetan Plateau & Polar Meteorology, Chinese Academy of Meteorological Sciences, Beijing, China.
[32]School of Earth and Space Sciences, University of Science and Technology of China, Hefei, China.
[33]Northwest Institute of Eco-Environment and Resources, Chinese Academy of Sciences, Lanzhou, China.
[34]College of Resources and Environment, University of the Chinese Academy of Sciences, Beijing, China.
[35]College of Geography and Environment, Shandong Normal University, Jinan, China.

Box 1 | **Tropical teleconnections and a bi-polar linkage**

Rossby wave dynamics operate in both the Northern Hemisphere and the Southern Hemisphere. Contemporary regional circulation and cryosphere changes in the Arctic and Antarctic are, therefore, synchronized to the same tropical sea surface temperature variability, specifically, that related to the Interdecadal Pacific Oscillation (IPO). For example, during 1979–2013, IPO-related cooling of the eastern Pacific is linked to bi-polar teleconnections, as observed by removing the zonal mean component from 200-hPa geopotential height trends (see figure). This global teleconnection consists of a two-pronged, large-scale Rossby wave train extending from the tropical Pacific to the North Atlantic and West Antarctic separately. There is evidence to suggest that this bi-polar linkage might represent a low-frequency internal mode in the climate system that recurred on multidecadal timescales over the past two millennia[265].

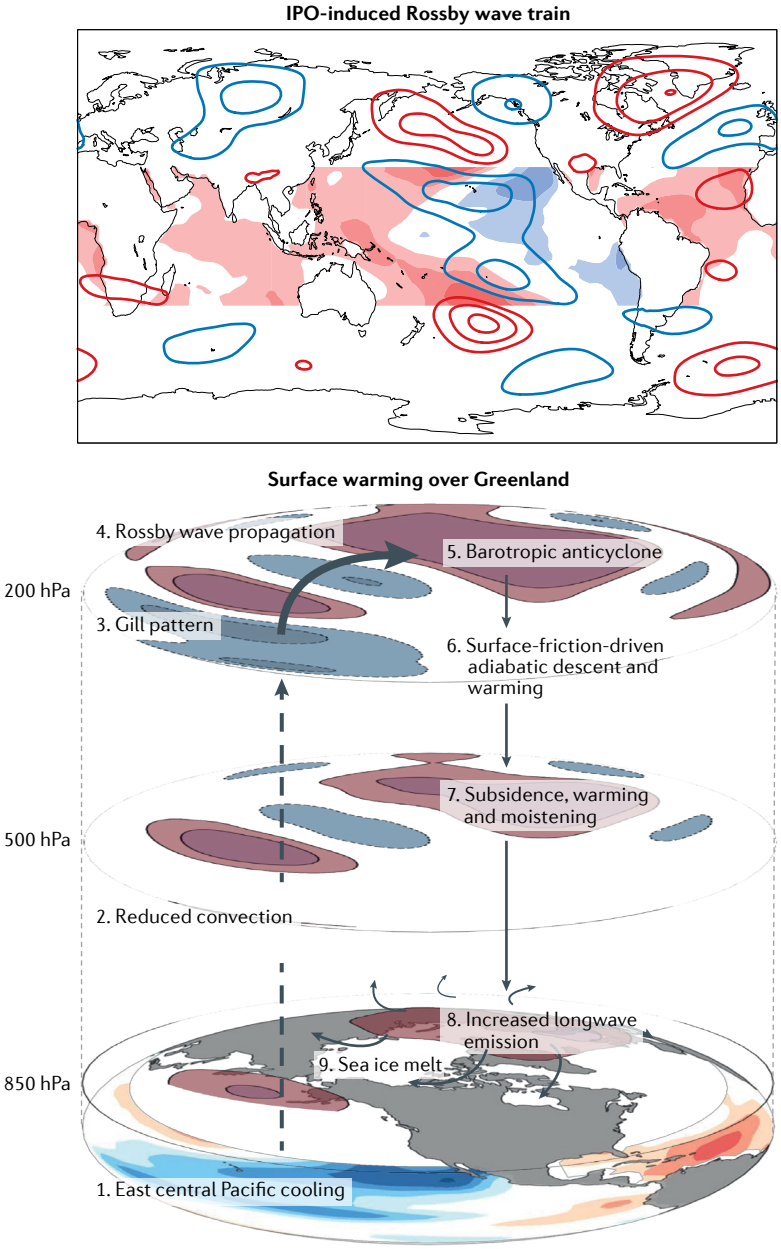

For the Northern Hemisphere, the IPO's transition to a cooling phase in the eastern Pacific triggered a Rossby wave train that extends from the tropical Pacific to the Arctic in a great arc, with a barotropic high-pressure system over Greenland (see figure). At the surface, friction causes anticyclonic winds to diverge, leading to downward movement of air to conserve mass. As the air descends, it adiabatically warms, allowing it to hold more moisture, and, therefore, increase low boundary cloud cover through increasing relative humidity below the inversion layer[266]. The combination of a warmer, cloudier and more humid atmosphere increases downward longwave radiation, contributing to surface warming and increased sea ice melt. Thus, owing to the location of pressure anomalies, the IPO has almost opposite impacts on the two polar regions, favouring climatic asymmetry between the Northern Hemisphere and the Southern Hemisphere[267].

Other tropical modes of variability, including the Asian summer monsoon[268–270], quasi-biennial oscillation[271] and Madden–Julian Oscillation[272,273], also drive anomalous Arctic circulation through stationary Rossby wave trains[268,272] and corresponding stratosphere–troposphere coupling[271]. These circulation anomalies have favoured contemporary sea ice melt via increases in temperature, humidity[268,271] and sea ice export.

(typically in the central tropical Pacific), triggering anomalous convective motion in the atmosphere[63]. This convection produces anomalous diabatic heating in the mid-troposphere and accelerates the local Hadley circulation, forming anomalous convergent flows at the descending branch that perturb the subtropical jet and generate an anomalous Rossby wave source in the subtropical upper troposphere. These wave sources subsequently excite a pattern of stationary Rossby waves[58,64,65], characterized by an anomalous low-pressure centre east of New Zealand, a high-pressure anomaly near the Amundsen Sea (thereby, interacting with the ASL) and another low-pressure centre over South America and the South Atlantic (FIG. 1a).

Amundsen Sea Low
(ASL). A climatological low-pressure centre located over the southern end of the Pacific Ocean, off the coast of West Antarctica, that exhibits substantial variability in strength, influencing the climate of West Antarctica and the adjacent oceanic environment.

El Niño–Southern Oscillation
(ENSO). An irregular periodic variation in winds and sea surface temperatures over the tropical Pacific Ocean on interannual timescales; the warming phase, El Niño, is characterized by anomalous warm sea surface temperature over the equatorial central-eastern Pacific, together with high and low surface pressure in the tropical western and eastern Pacific, respectively, and the cooling phase, La Niña, with generally opposite conditions.

Rossby wave trains
A series of cyclonic and anticyclonic vortices with a typical spatial scale of a thousand kilometres, superimposed on the uniform west-to-east flow, making up a succession of wave packages occurring at periodic intervals.

Antarctic Circumpolar Wave
Large-scale oceanic and atmospheric patterns, propagating eastward around the Southern Ocean with the Antarctic Circumpolar Current, on interannual and sub-decadal timescales. Features can be detected in sea level pressure, sea surface height, sea surface temperature and atmospheric/oceanic circulation.

Interdecadal Pacific Oscillation
(IPO). A climate mode describing changes in Pacific sea surface temperature on 20–30-year timescales; positive phases are characterized by an anomalous warming over the tropical eastern Pacific and cooling patterns over the extratropical–mid-latitude western Pacific.

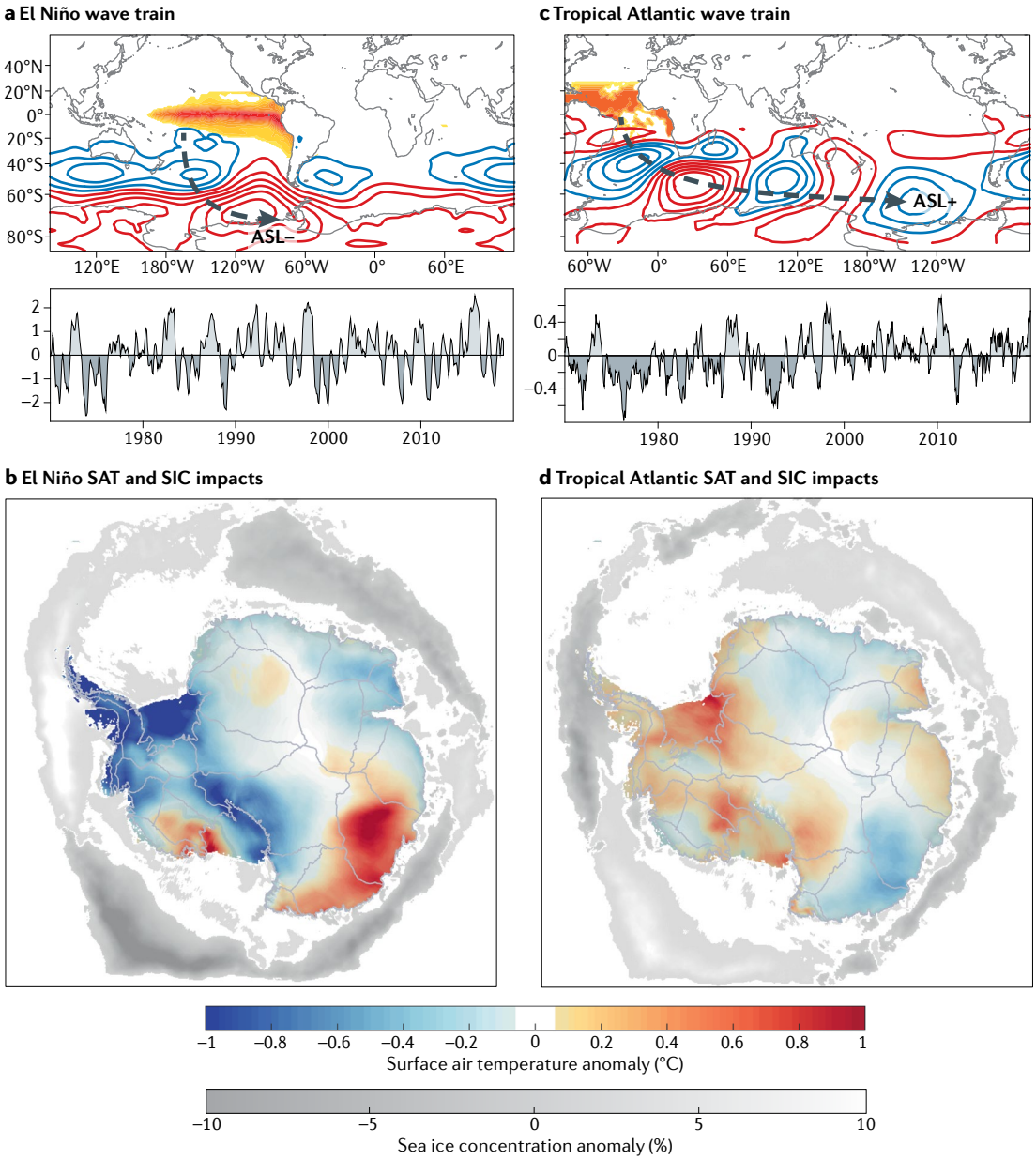

Fig. 1 | **Tropical–polar teleconnection patterns on interannual timescales. a** | Austral winter (June, July, August; JJA) 500-hPa geopotential height anomalies (contours) associated with equatorial Pacific warming (colour shading) in the atmospheric model, NCAR CAM5. The pattern of sea surface temperature anomalies represents a one standard deviation positive JJA El Niño–Southern Oscillation event. Red and blue contours indicate positive and negative pressure anomalies, respectively, drawn at intervals of 8 m. The time series is that of the Niño 3.4 index[259]. **b** | JJA Antarctic surface air temperature[260] (SAT) and sea ice concentration[261] (SIC) anomalies regressed onto the standardized JJA Niño 3.4 index; patterns represent anomalies associated with a one standard deviation El Niño event. **c** | As in panel **a** but for tropical Atlantic warming. The time series represents that of area-weighted mean temperature over the tropical Atlantic (20°S–20°N). **d** | As in panel **b** but regressions onto the tropical Atlantic time series. Both El Niño–Southern Oscillation and tropical Atlantic sea surface temperature variability promote stationary Rossby wave patterns to the Southern Hemisphere high latitudes; atmospheric pressure anomalies centred over the Amundsen Sea Low (ASL), in turn, drive SAT and SIC anomalies.

Atlantic Multidecadal Oscillation
(AMO). A climate mode that affects the sea surface temperature over the North Atlantic Ocean on multidecadal timescales, with an estimated period of ~60–70 years, and an amplitude of the spatial mean temperature up to 0.5 °C.

Hadley circulation
Vertical–meridional overturning atmospheric circulation over the low-latitude troposphere, characterized by rising motion near the equator, with air flowing poleward at the upper troposphere and descending over the subtropics.

Subtropical jet
A belt of strong upper-troposphere westerly winds in the subtropics, affecting precipitation and temperatures over the tropics and mid-latitudes.

The specific locations of these pressure centres depend on the location of the El Niño-related SST anomalies; that is, whether they are eastern Pacific or central Pacific El Niño events, describing peak SST anomalies at ~150°W–90°W and ~160°E–150°W over the equatorial Pacific, respectively. During a central Pacific event, there is a corresponding westward shift in locations where deep atmospheric convection can occur (regions with SST > 27.5 °C)[66]. As a result, Rossby wave sources for central Pacific events are also shifted westward by ~20°–30° relative to the eastern Pacific events[37,66,67]. In addition to being of opposite sign, anomalous SST and tropical convection during La Niña years occur to the west by 30–50° longitude, resulting in a corresponding westward shift of planetary waves relative to eastern Pacific El Niño years[68].

Waveguide
A certain layer of atmosphere, usually acted upon by the mean jet, in which the wave is trapped due to refraction, just as an electromagnetic wave propagates in a metal waveguide.

Thermal wind balance
The balance between vertical wind shear and horizontal gradients of virtual temperature in the atmosphere.

Walker circulation
Vertical–zonal overturning atmospheric circulation over the tropical belt; the dominant Pacific Walker cell is characterized by easterly winds at the lower troposphere, westerly winds at the upper troposphere, rising motion over the western Pacific and descending motion over the eastern Pacific.

It is only during austral winter, spring and autumn that such wave trains are able to propagate south. During these seasons, the strength of the subtropical jet is sufficiently strong and appropriately located to act as a waveguide[59,69,70]. During austral summer, in contrast, wave reflection by the background wind can hinder the ability of the wave train to reach the Amundsen Sea[71].

Mean atmospheric circulation dynamics

In addition to the Rossby wave response, ENSO signals can also be communicated to the polar regions by the atmospheric background circulation, and can involve both a zonally symmetric and a zonally asymmetric response in the SAM: the subtropical jet and the Hadley cell.

In the case of El Niño-related tropical Pacific heating, the zonally symmetric response results in an enhanced upper troposphere jet stream through eddy–mean flow interactions. However, the jet stream splits into the subtropical front jet (SFJ) and the polar front jet (PFJ) in the South Pacific, where the SFJ is strengthened and PFJ is weakened in response to El Niño events[72,73]. These conditions arise through the thermal wind balance between the tropical–subtropical region, as well as the balance in the vicinity of the mid-latitude to high-latitude eddy-driven mean meridional flows[41,42,45,70,74]. The converse occurs during La Niña-related tropical Pacific cooling; the SFJ weakens and the PFJ strengthens in the South Pacific.

As for stationary wave dynamics, the mean atmospheric responses are also influenced by the location of the Rossby wave source, and, further, by the location of El Niño-related SST variability. Specifically, while eastern Pacific SST variability projects strongly onto the SAM, only weak connections are apparent for central Pacific SST variability[66]. It is hypothesized that the relatively weak central Pacific El Niño-related SST anomalies are not able to substantially impact the subtropical jet and, thus, the SAM[66].

Zonally asymmetric responses to ENSO forcing are also observed in the mean meridional circulation over the Southern Ocean. In particular, during El Niño years, anomalous warming over the equatorial Pacific intensifies deep atmospheric convection, strengthening the Hadley cell in the tropical Pacific sector and leading to an equatorward shift of the subtropical jet[73,74]. By contrast, the El Niño-induced Walker circulation adjustment can cause subduction over the equatorial Atlantic Ocean, which relaxes and expands the Atlantic Hadley cell, accompanied by a poleward shift of the subtropical jet[73,75,76]. These zonally asymmetric Hadley cell responses between the Pacific and the Atlantic lead to different reactions of both the Ferrel and Polar cells, inducing asymmetric jet stream variations[73,75]. During El Niño, the subtropical jet strengthens and the polar jet weakens in the South Pacific[72,77,78], but in the South Atlantic, the subtropical jet weakens and the polar jet strengthens[73]. These changes alter the atmospheric blocking and storm distribution over the South Pacific, with an equatorward storm track shift and a corresponding reduction in storm activity over the Pacific sector[73,75].

ENSO-induced teleconnections might also influence the Ferrel cell through adjustment of the eddy fluxes. Atmospheric eddy activity intensifies the stationary waves, and ENSO signals have been observed in atmospheric transient eddies over the Southern Ocean[79,80]. ENSO variability alters storm tracks and, thus, impacts the regional Ferrel cell through adjustment of the convergence of meridional eddy heat flux[75]. The anomalous regional Ferrel cell further impacts Antarctic surface climate through modulation of the mean meridional heat flux[75].

Atlantic and Indian Ocean teleconnections

Stationary wave mechanisms operate not only in response to Pacific SST variability but also SST variability in other ocean basins, specifically, the tropical and northern Atlantic[28,65,81] (FIG. 1c). Anomalous tropical Atlantic warming, for example, can perturb atmospheric convection and intensify the local Hadley cell[65]. The downwelling branch of the intensified Hadley cell forms convergent flow in the subtropics, interacting with strong wind shear to trigger anomalous Rossby wave sources at the southern edge of the subtropical jet[59] (FIG. 1c). During austral spring, autumn and winter, strong anticyclonic curvature on the poleward flank of the jet reflects stationary Rossby waves. These conditions form a pathway from the subtropical Atlantic to the Amundsen–Bellingshausen Seas, focusing waves on the West Antarctic[55], where they act to deepen the ASL and drive a positive phase of the SAM[28,65] (FIG. 1c). In summer, however, the subtropical jet is too weak to trap the Rossby wave train and the teleconnection is no longer sustained[28,55,59,65].

In addition to the direct pathway, tropical Atlantic SST variability can also impact the Southern Hemisphere high latitudes through mediation of the Pacific[56,58]: Atlantic warming perturbs the zonal Walker circulation, creating anomalous convergent flow across the upper troposphere in the central and western Pacific. This anomalous convergence over the Pacific basin subsequently triggers a La Niña-like PSA pattern through Rossby wave dynamics, further deepening the ASL[58].

Similar to those from the Pacific and Atlantic basins, teleconnection patterns can also be generated by convective heating in the Indian Ocean. The Indian Ocean Dipole[20,57,82,83], for instance, can drive a Rossby wave train, propagating to high southern latitudes, influencing the Antarctic climate through its associated zonal wavenumber 3 pattern in austral spring[20,84]. Moreover, the Madden–Julian Oscillation, the principal mode of intraseasonal variability over the tropical Indo-Pacific Oceans, is further known to trigger Rossby wave trains that propagate to southern high latitudes[85–87], contributing to weekly-to-subseasonal variability in the SAM[88].

Impacts of teleconnections

Through the aforementioned mechanisms, especially stationary Rossby waves, Pacific and Atlantic SST variability can substantially impact interannual variability of the Antarctic atmospheric circulation.

An El Niño event typically leads to a weakened ASL, that is, an increase in sea level pressure of ~2–5 hPa (REFS[32,66,73]) (FIG. 1a), forming blocking highs frequently

South Pacific Convergence Zone
(SPCZ). A band of low-level convergence, cloudiness and precipitation extending from the Western Pacific Warm Pool at the Maritime Continent south-eastwards of the French Polynesia and as far as the Cook Islands (160°W, 20°S).

located around the Bellingshausen Sea[89]. The associated anomalous anticyclonic atmospheric circulation, and corresponding thermal and mechanical forcing, alters SAT and sea ice extent[32,37,66,73,90] (FIG. 1b). For example, during El Niño events, SAT over the Antarctic Peninsula can decrease by up to 1.5 °C, but increase by similar amplitudes over East Antarctica[66,73]. In turn, sea ice concentration increases by ~10–20% in the vicinity of the Amundsen, Bellingshausen and Weddell Seas, but decreases in the Amundsen and Ross Seas[66,73]. This pattern of anomalous sea ice extent is known as the Antarctic sea ice dipole[53] — the leading mode of ENSO-related Antarctic sea ice variability. El Niño years further tend to increase West Antarctic snow accumulation, owing to enhanced moisture transport into the region[15,91,92]. However, the weakening of the ASL also intensifies onshore flow of Circumpolar Deep Water (CDW) around West Antarctica[91], accelerating sub-ice shelf melting; ice dynamical effects outpace any mass gains from increased accumulation, resulting in overall mass loss. These impacts are strongly seasonal, with maximum sea ice anomalies occurring in austral spring when sea ice is in retreat[93,94].

Similar to ENSO-induced teleconnections, tropical Atlantic SST variability can also impact West Antarctic SAT and sea ice in austral spring through its impact on the ASL[28,65,81]. Tropical Atlantic warming typically deepens the ASL (FIG. 1c), heating the West Antarctic and Antarctic Peninsula, reducing sea ice, but increasing sea ice cover in the Ross Sea[28,65] (FIG. 1d). Given that the magnitude of SST anomalies in the Atlantic are lower than those in the Pacific, the amplitude of corresponding climatic anomalies is also weaker on interannual timescales. On decadal-to-multidecadal timescales, however, the Atlantic-induced teleconnection has marked impacts, which will now be discussed.

Multidecadal teleconnections

The time-averaged impact of interannual teleconnection mechanisms provides the basis for understanding decadal (or longer) changes in the Antarctic climate. In particular, since the late 1970s (when reliable satellite measurements began), annual mean sea level pressure of the ASL has deepened by ~1.4–3.7 hPa, depending on the reanalysis dataset used[36,95–97]. While the deepening of the ASL during austral summer is linked to an anthropogenically forced positive trend in the SAM[22], changes during other seasons have been linked to low-frequency tropical SST variability in the form of the IPO and the AMO[28,40,47,55,59,65].

The Interdecadal Pacific Oscillation and its teleconnection

The IPO features a spatial SST pattern reminiscent of ENSO but broader in meridional scale. In its positive phase, central and eastern equatorial Pacific SSTs are up to 0.5 °C warmer than average, whereas extratropical SSTs in the North and South Pacific are up to 0.5 °C lower than average, associated with an increase in the frequency of El Niño events[98,99] (FIG. 2a,b). These SST patterns typically persist for 20–30 years[98] (with ENSO events superimposed), and, therefore, have the capability to further modulate the amplitude and frequency of Pacific–Antarctic teleconnections[99].

From the late 1990s to ~2015, the IPO was in a negative phase[100]. Accordingly, negative SST anomalies in the central Pacific (FIG. 2b) — and corresponding changes in convection and upper-level vorticity — triggered a Rossby wave train similar to that observed during La Niña events: alternating patterns of high-pressure and low-pressure anomalies propagating south from the tropical Pacific, with a negative centre over the Amundsen and Bellingshausen Seas[99,101] (FIG. 2b). This anomalous Rossby wave train is robust for all seasons except austral summer, and could be partially attributed to the accumulation of a series of negative-phase PSA patterns triggered by La Niña events, whose frequency increased during the negative phase of the IPO[99,101].

In contrast to ENSO events, however, the IPO-related pressure anomaly pattern exhibits a stronger meridional gradient and greater zonal asymmetry over the South Pacific[47,101] (FIGS 1a,2b). These differences might partly arise from positive SST anomalies and subsequent convection in the South Pacific Convergence Zone[102] (SPCZ), known to trigger decadal-scale teleconnections through Rossby wave dynamics independent from those in the central equatorial Pacific[101,103]. These SPCZ-related wave trains result in an anomalous low-pressure centre in the Ross Sea. Thus, transitions and persistence of IPO-related SST anomalies and resulting wave train patterns allowed negative pressure anomalies to accumulate in the vicinity of the Amundsen and Bellingshausen Seas from the late 1990s through around 2015 (REFS[98,104]), intensifying the ASL by up to 4 hPa (REF.[47]) and driving decadal-timescale changes in atmospheric circulation.

The Atlantic Multidecadal Oscillation and its teleconnection

The AMO, sometimes referred to as Atlantic Multidecadal Variability, is the leading mode of decadal-scale Atlantic SST variability, with a periodicity of ~60–70 years[105]. In its positive phase, the AMO is characterized by positive SST anomalies over the North Atlantic. Spatially averaged SST anomalies total 0.5 °C, but local maxima of 2 °C are observed to the south of Greenland and in the tropical Atlantic (FIG. 2c).

Similar to the mechanisms described for interannual timescales, AMO-related SST variability is also able to impact Southern Hemisphere atmospheric circulation[28,58,65]. In all seasons but austral summer, positive AMO-related SST anomalies in both the north and the tropical Atlantic generate a stationary Rossby wave train, which propagates around the Southern Ocean, contributing to the negative pressure anomalies in the vicinity of the ASL (FIG. 2c). Since the transition of the AMO to a positive phase in the late 1970s, the AMO is believed to have contributed more than 50% of the total changes to the ASL from 1979 to 2012: ~3 hPa (REFS[55,59]).

Interbasin interactions

While the IPO and the AMO are known to influence trends in the atmospheric circulation over Antarctica, the impacts from individual basins are not linearly additive, owing to strong pantropical interactions[54].

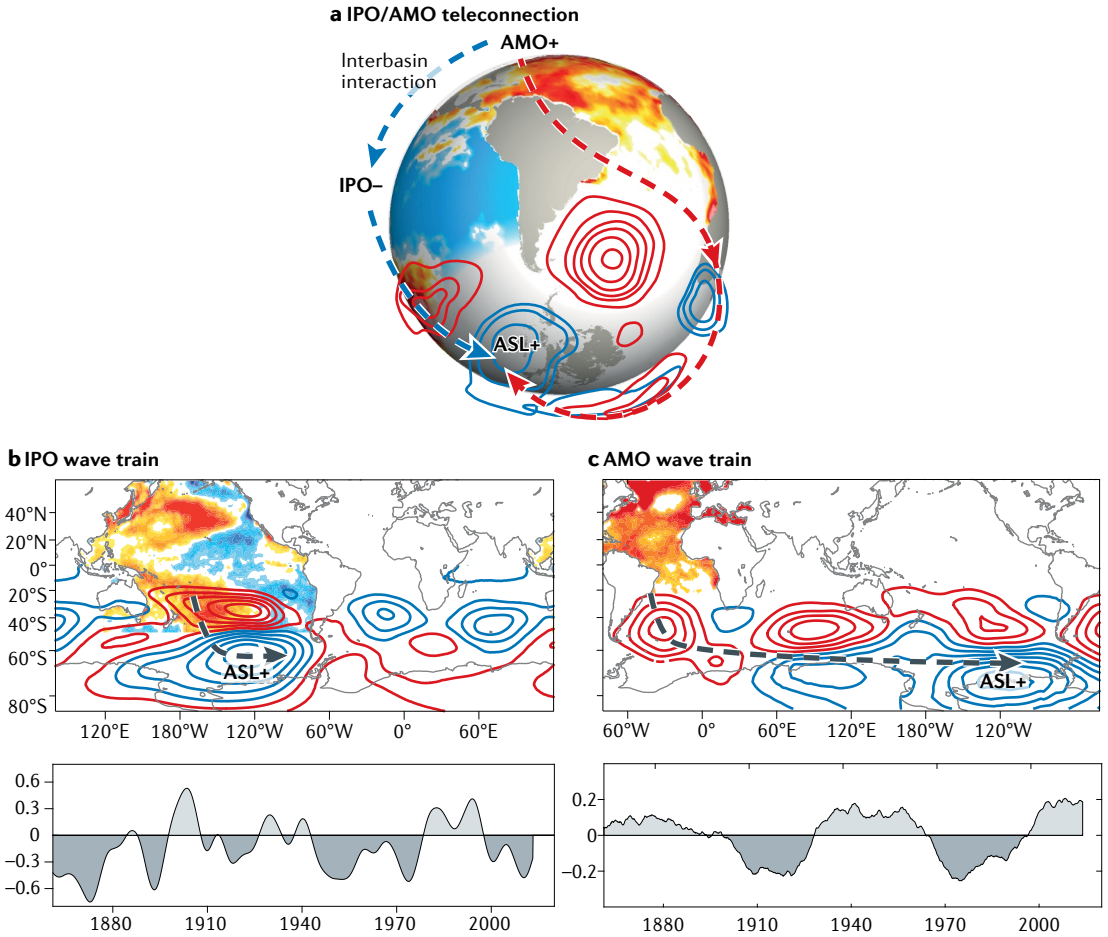

Fig. 2 | **Teleconnection patterns triggered by decadal sea surface temperature variability. a** | Schematic representation of the atmospheric teleconnection patterns induced by a positive phase of the Atlantic Multidecadal Oscillation (AMO; red arrow) and a negative phase of the Interdecadal Pacific Oscillation (IPO; blue arrow). **b** | Austral winter (June, July, August) 500-hPa geopotential height anomalies (contours) associated with a negative phase of the IPO (shading) in the atmospheric model, NCAR CAM5. The pattern of sea surface temperature anomalies represents a one standard deviation negative IPO event. Red and blue contours indicate positive and negative pressure anomalies, respectively, drawn at intervals of 8 m. The time series is that of the IPO index[98]. **c** | As in panel **b** but for a positive phase of the AMO. A positive phase of the AMO and a negative phase of the IPO both promote Rossby wave trains that deepen the Amundsen Sea Low (ASL). A positive AMO can also contribute to a negative phase of the IPO through interbasin interactions, complicating assessment of tropical–extratropical interactions.

For instance, Pacific SST variability has long been known to influence Atlantic SST variability[60]; equatorial Pacific warming during El Niño events typically warms the north tropical Atlantic, implying that the negative IPO phase could favour a cooling signal over the north tropical Atlantic. Moreover, the positive AMO could also have acted to intensify the observed negative IPO since the 1990s; anomalous atmospheric convection and Walker circulation responses to Atlantic warming lead to surface wind anomalies that cool the eastern tropical Pacific through wind–evaporation–SST effects, further reinforcing the negative IPO through the Bjerknes feedback[54,56,106]. The tropical Pacific and tropical Atlantic can, therefore, be mutually interactive, with each alternately influencing the other[107]. These interactions make it difficult to isolate the effect of each ocean basin, but, collectively, both have contributed to a deepening of the ASL (FIG. 2a), with corresponding impacts on the broader Antarctic climate.

Antarctic and Southern Ocean impacts

The AMO-driven and IPO-driven deepening of the ASL, in combination with the positive trend of the SAM, have contributed to a range of climatic changes surrounding Antarctica (FIGS 3,4).

Surface air temperatures

Substantial SAT changes have been observed across the Antarctic since the late 1970s (FIG. 4a–d). For instance, weak, statistically insignificant cooling is evident over East Antarctica (FIG. 4a,d), likely driven by a trend towards the positive phase of the SAM[21,108,109]. In contrast, rapid warming has been observed over West Antarctica[5,109–111] and the western Antarctic Peninsula[28] (FIG. 4a). In particular, Faraday/Vernadsky station (FIG. 4b), as an example of the western Antarctic Peninsula, experienced annual mean warming of ~2.8 °C from 1951 to 2000 (REF.[112]), with the trend in austral winter reaching ~5.6 °C per 50 years (REF.[28]). Over West Antarctica, the record at Byrd station

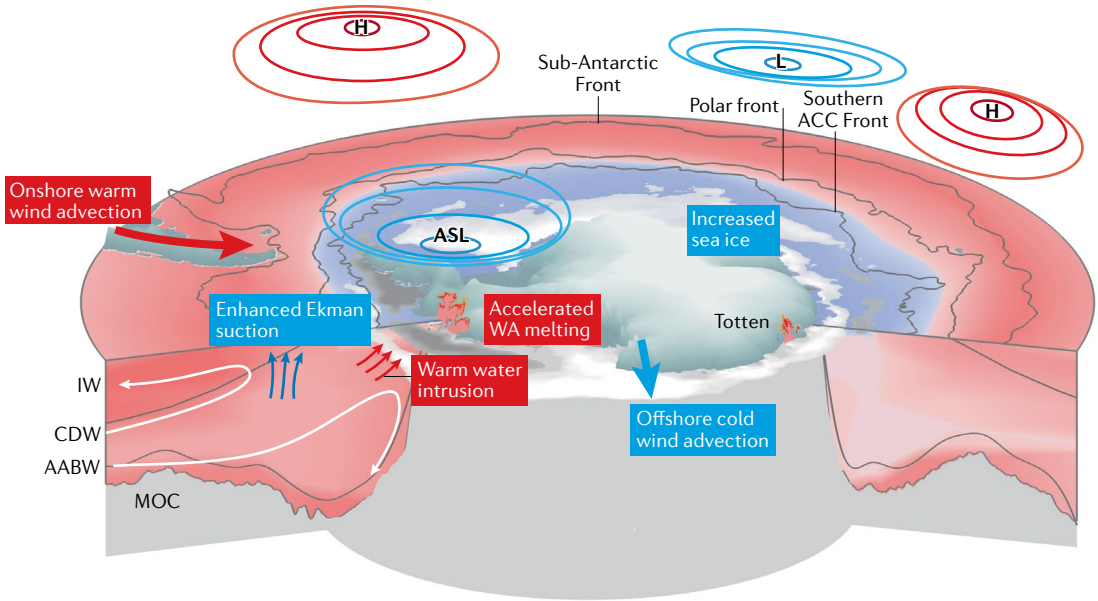

Fig. 3 | **Teleconnection-induced Antarctic climate changes.** Schematic depiction of Amundsen Sea Low (ASL) variability and corresponding impacts on the Antarctic climate, including temperature advection, sea ice redistribution, warm water intrusion and ice sheet melting. Red arrows and boxes indicate warming processes and impacts, and blue arrows and boxes indicate cooling processes and impacts. ASL variability can be linked to tropical teleconnections and anthropogenically induced changes in the Southern Annular Mode. AABW, Antarctic Bottom Water; ACC, Antarctic Circumpolar Current; CDW, Circumpolar Deep Water; H, high-pressure centre; IW, intermediate water; L, low-pressure centre; MOC, Meridional Overturning Circulation; WA, West Antarctica.

(FIG. 4c) reveals an increase in annual mean temperature of ~2.2 °C from 1958 to 2010 (REF.[4]). Moreover, a warming signal of ~0.6 °C per decade over the past 30 years is observed at the South Pole[113]. These warming signals are more than four times greater than the global average.

Such warming has been partly linked to decadal changes of ENSO[10,46,104], the IPO[47,64] and the AMO[28,55,65]. As noted, the transition of the AMO to a positive phase in the 1970s and the IPO to a negative phase in the early 2000s acted to deepen the ASL through stationary Rossby waves[28,47,59,64,65]. The resulting anomalous cyclonic circulation over the Amundsen Sea can, thus, in part, explain the increased SAT over West Antarctica via warm advection from the north[5,37,46,101,114,115] (FIG. 3). According to numerical simulations, for example, more than half of the observed West Antarctic warming can be attributed to teleconnection-induced ASL deepening[28,55]. Rapid warming over the Antarctic Peninsula[116] has further been linked to both teleconnection-induced thermal advection and an adiabatic compressional warming of air masses descending in the lee of the Antarctic Peninsula[28,65,104,117,118].

Since ~2000, many of these warming signatures over West Antarctica have shifted to cooling, as also apparent in the Antarctic Peninsula[112] (FIG. 4b,c). This temperature trend evolution is believed to be related to the eastward movement of the ASL and other remote forcings from the Pacific through the PSA wave train[112].

Sea ice

Sea ice paradox and redistribution. The total Antarctic sea ice extent trended upward slightly from the late 1970s until 2015 (REFS[97,119]) (FIG. 4e), with a total increase of ~1.1×10^6 km (REFS[10,120]). This positive trend counters what might be expected given the general warming of the global climate, and is opposite to the marked decrease in Arctic sea ice over the same period[121,122]. These hemispheric metrics, however, dilute strong regional variations in sea ice trends, specifically, decreases observed in the Amundsen and Bellingshausen Seas[123–126], and increases in the Weddell and western Ross Seas[74,93,96,127,128] (FIG. 4a).

As with SAT, the drivers of these sea ice changes are multifaceted and difficult to directly attribute to atmospheric circulation metrics[93]. Yet, while uncertainty remains, decadal variability of tropical SSTs, embedded in the AMO[28,31,55,58,59,65] and the IPO[8,47], are known to influence decadal variability of the SAM and the ASL, in turn, contributing to observed long-term sea ice changes[10,36,40,52,129]. In particular, the offshore wind associated with the ASL (FIG. 3) contributes to the formation of more sea ice over the Ross Sea through both cold atmospheric advection[28,39,130,131] and offshore ice drift[28,39,47,132,133]; onshore winds north of the Antarctic Peninsula conversely melt and compress sea ice around the coastal regions of the Amundsen and Bellingshausen Seas (FIG. 3). Notably, however, the impacts of the ASL on sea ice vary strongly with season because of the seasonality in the location of the ASL and the ice cover[129]. At a hemispheric scale, the importance of tropical teleconnections, specifically, the IPO, also become clear; during the negative phase (2000–2014), sea ice extent increased by $0.57 \pm 0.33 \times 10^6$ km^2 per decade, ~five times larger than the $0.12 \pm 0.11 \times 10^6$ km^2 per decade increase during the positive phase (1979–1999) (REF.[47]).

However, other factors have also contributed to observed sea ice trends, including: a zonal wave-three

pattern[134,135]; a series of regional air–ice–ocean interactions[136]; and freshwater fluxes associated with increased glacial melting[137], sea ice changes[18,26,138] and multidecadal convective cycles[27].

Post-2015 sudden sea ice loss. While Antarctic sea ice extent increased up to 2015, even in a warming climate, a rapid reduction has been observed thereafter[9,139] (FIG. 4e,f). In March 2016, Antarctic sea ice extent decreased by ~2.25×10^6 km^2 relative to its climatological value[12], and subsequently dropped to its lowest extent on record in March 2017, 2.07×10^6 km^2.

This sudden decrease has been largely attributed to changes in near-surface wind forcing. Numerical experiments[140], for instance, indicate that wind-driven sea ice changes capture the majority of the observed sea ice loss from 2014 to 2016, with atmospheric teleconnections contributing to these near-surface wind changes[8,11,139,141]. The transition to a positive phase of the IPO in ~2014–2016 (REFS[8,142,143]), in particular, influenced these surface wind anomalies via the resulting teleconnections, interacting with other processes to produce sudden sea ice loss[8,20].

These other processes include a persistent zonal wavenumber 3 pattern, partially induced by the remote forcing from a record negative Indian Ocean Dipole[20,139,141], and a near-record negative value of the SAM index in November 2016 (REFS[11,12]), linked to tropical Pacific SST anomalies. Moreover, an intensified ocean vertical heat transport[8], and a reoccurrence of the Maud Rise polynya (possibly associated with the Southern Ocean internal multidecadal variability[27]), are also believed to have influenced the sudden sea ice loss in 2016, highlighting the complexity of the potential mechanisms driving the contemporary Antarctic sea ice changes.

Southern Ocean

Warming and oceanic heat content. The subsurface Southern Ocean has warmed in the upper 2,000 m since the 1950s (REFS[2,144–149]), as also evidenced by Argo data from the early 2000s to 2016 (REF.[8]) (FIG. 4g) and regional sea level trends[150,151]. While largely attributed to anthropogenic forcing[144,152], this warming is also associated with enhanced Ekman pumping around 40°S–50°S driven by the positive phase of the SAM[23,153], in turn, partially forced by the positive phase of the AMO[28,65].

Superimposed on these long-term trends is shorter-term variability. In particular, the combination of the IPO phase transition in 2014–2015 and a negative SAM in 2015 weakened surface westerlies over the Southern Ocean[8,140]. Along with a preponderance of anomalous surface northerlies (also resulting from teleconnections with the tropical oceans) and consequent warm air advection towards Antarctica[139], the upper layer (above 400 m) of the Southern Ocean became anomalously warm from 2016 (REF.[8]).

South of the Antarctic Circumpolar Current, prior to 2016, the surface waters had generally cooled slightly[99,144,154] (FIG. 3). In the Bellingshausen Sea, the increase in atmospheric temperature warms the upper ocean in summer[155], associated with a subsurface warming within the CDW[34,156–158]. In the Amundsen Sea, the CDW layer thickness has varied dramatically along the continental shelf, with an approximately decadal period, in response to tropically driven variability in wind forcing[15,92,159–161]. Around Antarctica, the CDW off the continental shelf experienced a long-term warming, partly driven by a surface ocean freshening through sea ice and glacial melting[138,162].

Changes in salinity. Concurrent with warming of the lower latitude subsurface Southern Ocean[152] is a freshening along the coast[163,164] and in the open ocean[164,165], particularly at the surface and in Antarctic Intermediate Water[145,166–168]. The regional decrease in salinity has been attributed primarily to a wind-driven increase in northward transport of sea ice from the Antarctic coast to the open ocean[18], an increased freshwater flux from Antarctic glacial melt[169] and increased precipitation over evaporation[165]. For example, over the Ross Sea, the southerlies and westerlies have strengthened, contributing to freshening in the open ocean[18]. These near-surface wind changes are associated with deepening of the ASL. The deepened ASL also contributed to anomalous ocean heat and salinity fluxes through its adjustment of the Ross Gyre[170] and Subantarctic Mode Water[171].

Land ice

Improved airborne and satellite remote-sensing measurements and analysis techniques have allowed for a more accurate quantification of changes in the mass of the Antarctic ice sheet. Estimates of ice sheet mass change agree with each other to within their uncertainties and consistently capture two distinctive features: an acceleration in Antarctic ice sheet mass loss over the last 25 years[16,29,172] (FIG. 4h–j) and overall mass loss dominated by that from West Antarctica and the Antarctic Peninsula[29,33,35] (FIG. 4a).

The Antarctic ice sheet lost 2,720 ± 1,390 Gt of ice between 1992 and 2017 (REF.[29]). The largest cumulative mass losses occurred in West Antarctica and the Antarctica Peninsula, which, over the period 2012–2017, reached 159 ± 26 Gt per year (72% of total) and 33 ± 16 Gt per year (15% of total), respectively[29]. The biggest mass reductions are evident in the Pine Island Glacier (FIG. 4a,j) and Thwaites Glacier (FIG. 4a,i) catchments of the Amundsen Sea Embayment[173,174], and along glaciers feeding recently collapsed or rapidly thinning Larsen ice shelves[175,176].

In contrast, the East Antarctic ice sheet exhibited an insignificant mass loss or even an ice gain[6,29], although regional mass loss is evident at the Totten Glacier since the 2010s[177] (FIG. 4a,h). This strong asymmetry between land ice changes in East versus West Antarctica could be associated with atmospheric and oceanic circulation changes driven by tropical–polar teleconnections.

Since the 1990s, mass loss from the West Antarctic ice sheet — focused in the Amundsen Sea Embayment — has dramatically accelerated[6,29,173]. This acceleration is primarily the result of increased sub-ice shelf melting and thinning[6,172,173,178], the loss of ice shelf buttressing[179] and a resulting increase in the flux of grounded ice upstream[180–182]. Both observations and modelling

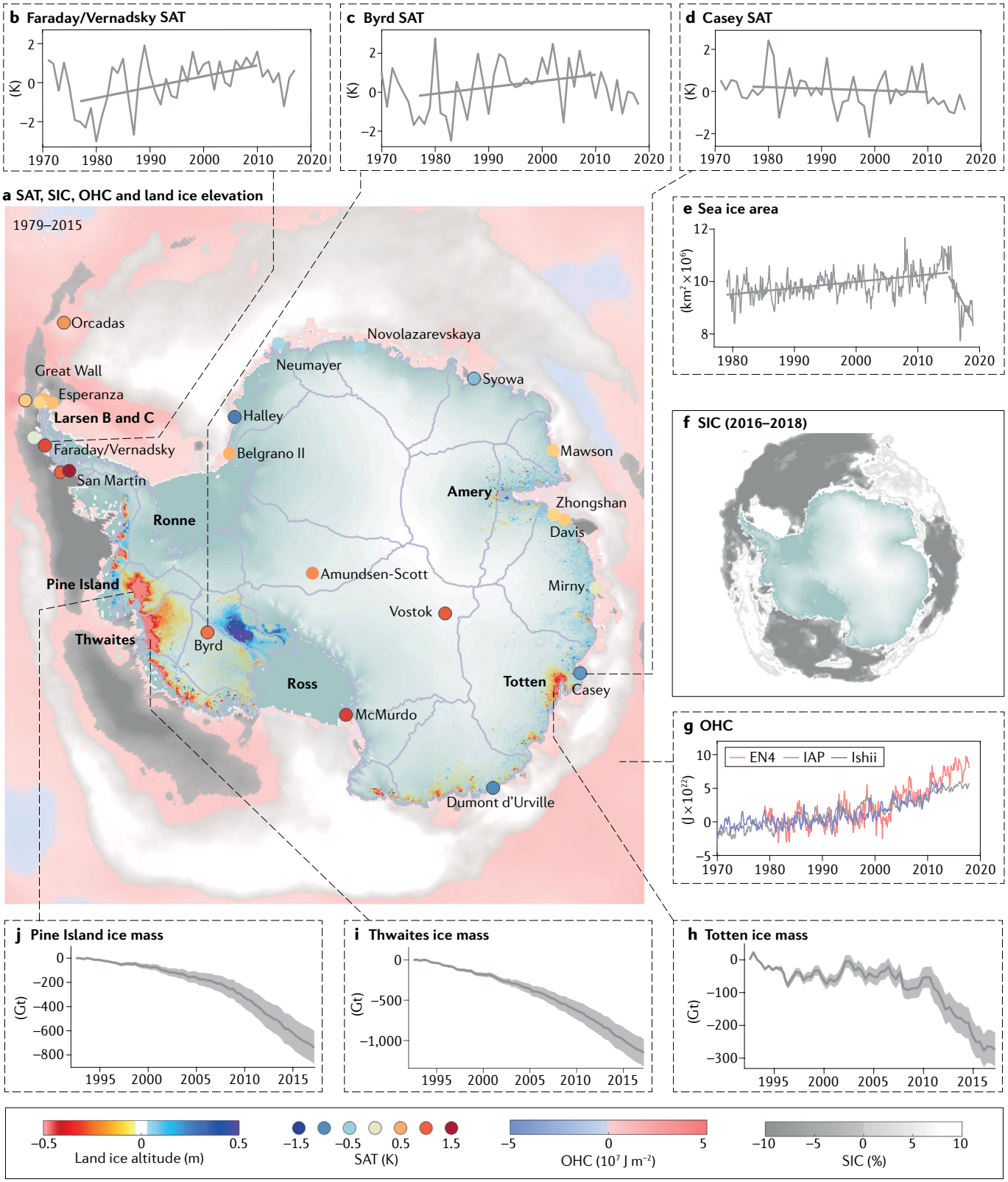

indicate that variability in sub-ice shelf melting is related to periodic incursions of CDW onto the continental shelf in the Amundsen Sea Embayment[15,160]. These incursions are primarily associated with eastward zonal wind anomalies at the shelf break[15,160,161,183,184], linked with anomalous atmospheric circulation of the ASL driven by Pacific[15,91,92,135,159,160] and Atlantic decadal variability[28,65]. Models experiments suggest that anthropogenic forcing has driven a gradual westerly wind trend during the twentieth century, leading to a gradual increase in the strength and duration of CDW incursions onto the Amundsen Sea shelf[159].

◀ Fig. 4 | **Observed climate changes around Antarctica. a** | Observed annual-mean trends in ice sheet elevation[174] (coloured shading within the continent), surface air temperature[260] (SAT; coloured circles), ocean heat content[262–264] above 1,500 m (OHC; shading over the ocean) and sea ice concentration[261] (SIC; white-grey shading surrounding the continent). Trends are calculated over 1979–2015, except for ice elevation, which are over 1992–2017. **b** | Time series (1971–2018) and trend line (1979– 2010) of annual mean SAT at Faraday/Vernadsky station, Antarctic Peninsula. **c** | As in panel **b** but for Byrd station, West Antarctica. **d** | As in panel **b** but for Casey station, East Antarctica. **e** | Time series of hemispheric monthly mean sea ice area (seasonal cycle removed); trend lines are illustrated for 1979–2015 and 2016–2018. **f** | Spatial pattern of SIC from 2016 to 2018. **g** | Time series of monthly mean Southern Ocean (south to 35°S) heat content anomalies above 1,500 m from three independent datasets. **h** | Time series of monthly mean Totten Glacier ice mass loss. Shading represents mass balance uncertainty. **i** | As in panel **h** but for Thwaites Glacier. **j** | As in panel **h** but for Pine Island Glacier. In the four decades since 1979, substantial climate changes have been observed in the Antarctic, including rising SAT and thinning ice sheet in West Antarctica, a general Antarctic-wide sea ice expansion followed by a rapid sea ice loss after 2015 and a basin-wide increase of the OHC in the Southern Ocean. Most of these changes feature zonal asymmetric patterns, with the strongest changes around West Antarctica.

Like the Amundsen Sea Embayment, glaciers on both sides of the Antarctic Peninsula have experienced increased dynamic mass loss following thinning and collapse of peripheral ice shelves[176,185–187]. Multiple processes could contribute to this change, including surface melting and hydrofracture[188] as a result of increasing SATs, atmospheric blocking and longwave downwelling[175], increased sub-ice shelf melting[156,189] and increased vulnerability to ocean wave impacts from reduced sea ice in the Bellingshausen and Weddell Seas[163,190]. Surface and ocean warming and regional sea ice reductions in this region are all tightly linked to tropical SST variability, indicating teleconnections between tropical climate variability and observed increases in Antarctic Peninsula ice mass loss.

Although several lines of evidence from observations and numerical simulations[15,91,159,161,175,184] link tropical ocean variability to Antarctic ice sheet mass change, the integrated impacts result from the net effect of atmospheric[15,28,65,92] and oceanic dynamical processes[15,92,160,161], coupled sea ice–ocean–atmosphere interactions[28,47,136,159] and ocean–ice shelf interactions[15,160,191], making it difficult to quantify the effect of specific teleconnections on Antarctic ice sheet mass balance. In particular, limited understanding of, and limited ability to model, the physical processes acting beneath and at the fronts of ice shelves[15,184,192–194], in turn, limit the ability to simulate and better understand their connections to tropical climate.

Implications for global climate

Antarctic changes and decadal variability have broad impacts on global climate, including vertical ocean heat and salinity exchange, the overturning circulation, the carbon cycle and global sea level. These changes could be further influenced by teleconnections from the tropics.

The enhanced vertical salinity[18] and heat[138,195] transport between the surface and deep Southern Ocean is associated with the redistribution of Antarctic sea ice[18,138], which might, in part, result from tropical–polar teleconnections[8,28,65,196]. Salty, dense shelf water sinks to the bottom of the Southern Ocean, contributing to the formation of Antarctic Bottom Water[17,19,196] and serving as a major contributor to the global overturning circulation[197]. Contemporary sea ice changes also intensify Southern Ocean stratification[18], weakening the mixing and upwelling of deep water to the surface, which can influence the net CO_2 uptake of the Southern Ocean[198,199].

The increase in Southern Ocean heat content and melting of the Antarctic ice sheet have contributed to both regional and global sea level rise over the last three decades. On the continental shelf, sea level trends reflect increased freshwater supply from the ice sheet[200]. However, they are also consistent with increasing ocean heat content, with the fastest rate in the south-east Indian Ocean and slight decrease in the Pacific sector of the Southern Ocean, consistent with the positive SAM pattern[150,151]. Since 2005, Southern Ocean heat content increased faster than any other ocean basins[201,202], contributing to more than 67% of global mean thermosteric sea level rise[147,202]. Meltwater from the Antarctic ice sheet contributes to the global ocean mass-equivalent sea level rise. Since 1993, the era of satellite observations, the Antarctic ice sheet experienced dramatically accelerated mass loss[203], contributing an annual rate of sea level rise of 0.14 ± 0.19 mm per year during 1992–1997 and increasing to 0.61 ± 0.12 mm per year during 2012–2017 (REF.[29]). The tropical-Pacific-induced near-surface wind impacts on regional sea level changes over the Southern Ocean contributed to variability of the Antarctic Slope Current and the Ross and Weddell Gyres[204].

The importance of anthropogenic forcing

Anthropogenic forcing also plays a fundamental role in driving climate changes around the Antarctic. Ozone loss and its recovery after the early 2000s are the primary drivers of the decadal trend and variability of the SAM[22,23], especially during the austral spring and summer, and increased GHG concentrations can similarly intensify the polar vortex[25]. Both factors contribute to a poleward intensification of the oceanic subtropical gyres of the Southern Hemisphere[24,205], intensifying Ekman pumping over the Southern Ocean and altering the Antarctic surface climate[22,23,25]. While teleconnections from the tropics explain a considerable fraction of the zonally asymmetric patterns of Antarctic climate change, GHG increases and ozone changes are more strongly associated with the symmetric part of the observed circulation changes, according to model simulations[23,25].

Projected teleconnection changes

Having established the impact of tropical climate variability on the Antarctic ocean–atmosphere system, future anthropogenically forced changes in the mean state circulation can be anticipated to modulate projected teleconnections and their responses. In many instances, these projections are hypothetical or remain inadequately explored with regard to direct extratropical impacts and, in particular, when considering their compounding influences. However, they offer some insight into how observed multidecadal SST variability in the tropics

could change, and, therefore, what related perturbations to Antarctic climate might be expected.

Tropical circulation and variability

The tropical mean climate is anticipated to undergo substantial changes as a result of anthropogenic warming[206,207]. In particular, owing to the projected slowdown of the Pacific Walker circulation, tropical eastern Pacific SSTs are projected to warm faster than those of the western Pacific. For instance, in $2\times CO_2$ simulations, the projected anomalous SST over the equatorial eastern Pacific can be ~0.5 °C warmer than that over the western Pacific[206]. Through the aforementioned teleconnection mechanisms, this El Niño-like change could result in a weaker ASL conducive to negative sea ice anomalies in the Ross Sea, positive sea ice anomalies in the Amundsen and Bellingshausen Seas and greater ice sheet surface accumulation over West Antarctica[91].

Other changes are also anticipated to the tropical circulation, although the impact on teleconnections is unclear. For instance, faster warming is expected in the equatorial zone compared with the off-equatorial Pacific. As a consequence, an equatorward shift of the Pacific Intertropical Convergence Zone and the SPCZ are anticipated (even if SST variability does not change), as convergence zones tend to follow maximum surface temperatures[84,208]. An increase in ocean–atmosphere coupling — linked to intensified stratification of the upper ocean[207] — is further likely to enhance El Niño SST variability, despite being strongly modulated by internal variability[209–212]. Increased occurrences of extreme El Niño events, in turn, lead to more frequent extreme La Niña events[207], as the discharge following an extreme El Niño shallows the thermocline basin-wide[213], allowing for a stronger subsurface influence on SST. Despite an absence of inter-model consensus[214,215], strong and concentrated convection is similarly likely to become established in the western Indian ocean, leading to an increased frequency in extreme positive Indian Ocean Dipole events[84,216].

While there is an absence of direct quantification, under continued GHG warming, it can generally be expected that teleconnections to the Antarctic region via the stationary Rossby wave (the PSA pattern) are likely to intensify with a slight eastward shift[217–224] (FIG. 5).

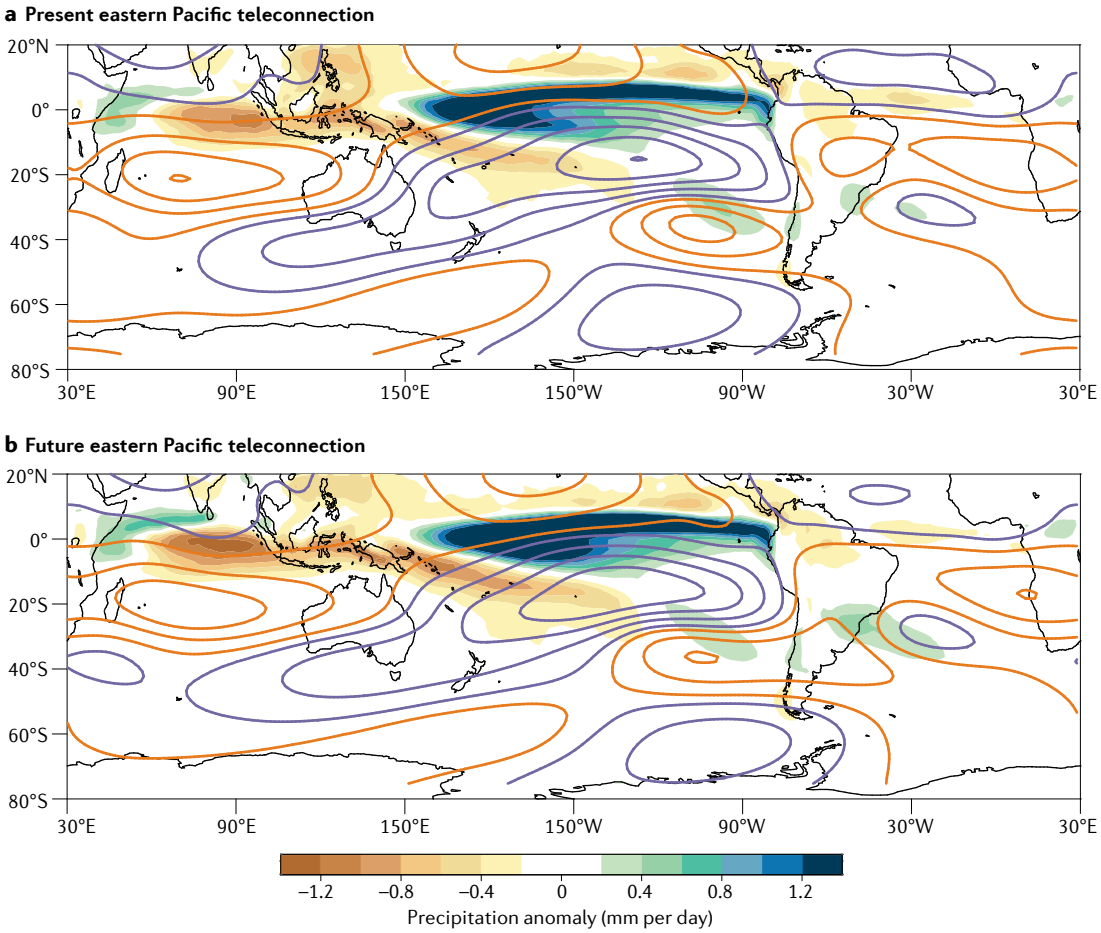

Fig. 5 | **Present-day and future eastern Pacific teleconnections. a** | Present-day (1900–1999) multi-model mean September, October, November rainfall (shading) and 200-mb stream function (contours) anomalies regressed onto September, October, November eastern Pacific El Niño–Southern Oscillation (ENSO) index. Orange and purple contours indicate positive and negative stream function anomalies, respectively, with a 0.75×10^6 contour interval. Multi-model ensemble consists of 17 CMIP5 models that realistically simulate ENSO non-linearity[212]. **b** | As in panel **a** but for future projections (2000–2099) under a high CO_2 emission scenario (RCP8.5). ENSO-induced teleconnections are projected to intensify with a slight eastward shift.

Multidecadal variability

In the coming decades, the phases of the AMO and the IPO might reverse, modifying their corresponding teleconnections and adjusting asymmetry associated with ASL variability. Specifically, if the IPO were to transition to a positive phase (as has been suggested to have occurred around 2015 (REF.[47])) and if the AMO were to transition to a negative phase (as anticipated in the next three to four decades), the joint impact would be a shallowing of the ASL. That is, their combined influence would drive positive trends in the geopotential height of the ASL, producing a circulation response opposite to that observed since the 1970s (REFS[28,40,47,65]) (FIG. 2). As a result, East Antarctica could undergo a more severe warming and experience faster melting than observed to date, potentially accompanied by surface cooling (or decreased warming) over the Antarctic Peninsula and West Antarctica, a decrease in sea ice over the Ross Sea and a relative increase in sea ice cover in the Amundsen and Bellingshausen Seas. However, given the complexities in the teleconnection patterns and decadal ocean variability, as well as the large uncertainties in future projections under anthropogenic forcing, it remains to be seen how the superposition of these AMO and IPO phase changes will influence the sign and magnitude of climatic changes in Antarctica.

While the natural cyclicity of the IPO and the AMO will inevitably influence their Antarctic teleconnections, anthropogenic warming is also anticipated to influence the AMO and the IPO directly[225,226]. In particular, projected strengthening of upper ocean stratification in the Pacific and Atlantic, although conducive to the growth rate of these modes, is thought to lead to faster propagation of oceanic Rossby waves. The acceleration of Rossby waves, together with a slowdown of the Atlantic Meridional Overturning Circulation, reduce the intensity of the IPO and the AMO by up to 60% and shorten their periods[225–227], leading to a weakened teleconnection pattern between the tropics and the Antarctic climate on decadal timescales. However, a reduction in the Atlantic Meridional Overturning Circulation might conversely reduce warming in the tropical Atlantic, and, therefore, the warming differential between the tropical Atlantic and Pacific, with the result that teleconnections trend towards those associated with a positive IPO.

A changing ambient circulation

The impact of teleconnections in the future could also be modified by changes in the mean ambient circulation. Under GHG warming, a poleward expansion of the Hadley cell[228] and a poleward intensification of mid-latitude westerly winds manifests as a trend towards positive phases of the SAM[23,24,229,230]. These projected changes would cause a spinup and southward strengthening of the subtropical gyres — a southern mid-latitude interbasin flow from the Great Australian Bight to the Indian Ocean and the Atlantic[231] — bringing warmer water closer to the Antarctic region. At higher latitudes, the intensified westerlies would lead to greater storage of heat in the Southern Ocean[230,232] by intensifying the process of heat uptake; upwelled subsurface water would be heated by atmospheric warming, transported northward by Ekman transport and subducted into the deep ocean along isopycnic surfaces. Although Antarctic ozone recovery would offset the impact from increasing GHG emissions, the positive SAM-like changes and associated heat uptake could accelerate in the post-ozone recovery period[24,233].

Summary and pathways forward

Through Rossby wave dynamics, multidecadal SST variability in the Atlantic and Pacific Oceans has strongly influenced the Antarctic climate since the late 1970s. Deepening of the ASL and the positive SAM trend — partly related to phase changes in the IPO and the AMO, and the accumulation of their teleconnection responses — has caused thermal and mechanical forcing that contributes to zonally asymmetric trends observed over Antarctica (FIGS 3,4). These include CDW warming in the Southern Ocean, an increase in the total sea ice extent before 2015 and a sudden sea ice loss thereafter, and impacts on ice sheet thinning around West Antarctica. Similar tropical–polar teleconnections are also evident on longer timescales, as revealed by palaeoclimate records (BOX 2).

These influences have important implications for understanding and projecting future changes in Antarctica, but substantial uncertainties exist in understanding contemporary and future systems. For instance, the relative importance of tropical–polar teleconnections, anthropogenic forcing and internal variability are still not fully understood. With this recognition, we discuss priorities for future research.

Sustained observations

Given the timescales involved, many tropical–polar teleconnections last for decades or longer[28,40,47,58,65]. Their investigation, thus, requires long-lasting and concurrent measurements. However, while sporadic observations are available, sustained (or any) observations over Antarctica are largely missing. One example is the sparsity of subsurface ocean monitoring to better elucidate the causes and the impacts of warm water intrusions[34,234]. Moreover, where observations do exist, they are often highly uncertain, for example, the remote-sensing observations of Antarctic surface temperature trends and ice loss[29,172,173,235]. Quantifying long-term teleconnections, therefore, necessitates long-term observations from both the tropics and the high latitudes, in particular, observations of the Antarctic atmospheric and oceanic circulation, temperature, precipitation, sea ice concentration and thickness, as well as the mass and energy budgets; they are presently lacking both spatially and temporally.

Yet, launches of a series of polar orbiting satellites[236], under ice and deep ocean Argo floats[237,238], autonomous underwater vehicles[239] and deployment of hundreds of automatic weather stations[240] facilitate the monitoring of meteorological conditions and environmental changes around the entire Antarctic region. Image recognition and machine learning techniques are also being used to better evaluate ice sheet and ice shelf dynamics[241]. Nevertheless, an urgent need persists to produce a long-lasting, full-coverage, multivariable dataset of the atmosphere, ocean, sea ice and land ice by combining existing satellite,

Box 2 | **Palaeoclimatic tropical–polar teleconnections**

Given the prevalence of tropical–Antarctic teleconnections in modern climate, it is prudent to consider whether such relationships also exist in the past and whether they have influenced long-term global climate change.

Over the past couple of millennia, variability originating from the tropical Pacific appears sufficient to explain both decadal variance and trends in water isotope proxy records from across West Antarctica[274]. During the last glacial period, there is interest in whether drastic changes in mean climate — including a 3–4 °C cooler climate than the present day[275] — influenced changes in El Niño–Southern Oscillation (ENSO)-related tropical variability[276,277]. Palaeo-proxy evidence for such an influence is mixed, however, and complicated by the possibility that ENSO's influence in regions outside the tropics might change with mean state[278–280].

A high-resolution, ice-core water-isotope record from West Antarctica additionally suggests that ENSO-related interannual and decadal variability in the Amundsen Sea Low was a factor of two larger during the last glacial period than compared with the present-day climate[281]. Further, variability declined abruptly 16,000 years ago, coincident with the deglaciation of the Laurentide–Cordilleran ice sheet in North America. The topographic presence of the large Laurentide–Cordilleran ice sheet altered the atmospheric circulation in the tropical Pacific, in turn, influencing the Rossby wave train between the tropics and the Amundsen Sea Low[281]. Regardless of whether the variance of ENSO itself changed, its influence on the climate in West Antarctica was significantly greater during the last glacial period, owing to the presence of Northern Hemisphere ice sheets and their amplification of the teleconnection mechanism.

Before the last deglaciation, the last glacial period was punctuated by millennial-scale climate variability, known as Dansgaard–Oeschger (DO) oscillations, consisting of large and abrupt warming events in the North Atlantic region, along with muted, out-of-phase temperature changes in the Antarctic[282–284]. The abrupt changes in interhemispheric temperature asymmetry associated with these warming events can alter the tropical atmosphere, shifting the Hadley cells towards the anomalously warm hemisphere, to help satisfy the global energy balance through cross-equatorial heat transport[285]. A range of palaeo-proxy evidence suggests abrupt latitudinal shifts in the Intertropical Convergence Zone and tropical hydrology during DO events[286–288]. These changes in tropical atmospheric circulation can impact the Antarctic by rapidly shifting the latitudinal position of the Southern Hemisphere westerly winds and storm tracks, either through zonal-mean[289] or Pacific-centred teleconnections[290].

Water-isotope records from Antarctic ice cores have demonstrated synchronous, systematic shifts in moisture origins linked to changes in storm track position during DO events, within decades of both the abrupt changes in tropical atmospheric circulation and abrupt changes in Northern Hemisphere climate[291]. While first identified in the Pacific sector of Antarctica[291], evidence for these tropically forced westerly wind shifts has since been found in all sectors of the Antarctic[292]. Furthermore, these signals linked to tropical atmospheric teleconnections are detected in Antarctica a century or more before signals tied to ocean circulation changes during DO events[291,292]. By changing poleward atmospheric heat transport[293] and/or influencing the carbon cycle via Southern Ocean ventilation[294], these atmospheric teleconnections might have an active role in the dynamics of millennial climate variability and drive changes in Southern Hemisphere temperature, which is otherwise largely thought to be dominated by changes in ocean circulation.

ship, Argo float and ground-based observations, in order to more systematically study Antarctic climate variability and the associated tropical–polar teleconnections.

Climate model improvement

Compensating for insufficient observations, climate models are a vital tool for understanding the mechanisms and impacts of tropical–polar teleconnections and for projecting future changes. However, models are often inadequate in many respects, necessitating efforts for improvement. For example, ice shelf–ocean interactions are only just starting to be included in some contemporary climate models[193], preventing an accurate assessment of future sea level rise under GHG-induced warming, including the contribution from tropical teleconnections. Several key physical processes are also not well represented, owing to coarse resolution and inadequate parameterizations. Examples include: the impacts of ice shelf calving[192,194]; CDW intrusion under the Antarctic shelves and related feedbacks[15,160,191]; atmosphere–sea ice–ocean interactions[136]; and the radiative effect of clouds over the Southern Ocean[242]. In addition, there are substantial model biases in representation of the mean flow of the polar atmosphere, and the mean state and variability of the tropical oceans, including an equatorial Pacific cold tongue bias[243], an inability to simulate observed ENSO diversity[212] and underestimated Atlantic forcing of the IPO (or forcing from the Pacific on the AMO) and associated teleconnections to the Antarctic region.

These biases and uncertainties in state-of-the-art climate models hinder the accurate simulation of the mechanisms, impacts and projections of tropical teleconnections to the Antarctic. In particular, they limit the ability to quantify climate impacts of teleconnections from different ocean basins. Improvement of models in the context of a fully interactive Earth system framework and involving a hierarchy of high-resolution atmosphere, ocean and ice components with substantial reductions in major biases is an important pathway to progress. In addition, the use of advanced modelling techniques including pacemaker simulations[56,107,141,244] and large-ensemble experiments[115,245] can aid in the understanding of mechanisms and uncertainties related to tropical–polar teleconnections.

Improved understanding

With better observations and models, progress can be made towards answering several key questions regarding tropical–polar teleconnections.

First, while the influence of the tropics in explaining climate variability and change in Antarctica has been established, the relative role of anthropogenic forcing[21–23,206], regional climate variability and tropical teleconnections[10,28,53,58,65] remains unclear. Better knowledge of their contributions will facilitate better understanding of future Antarctic projections, and, so, should be a major focus of future research.

Second, owing to inadequate observations, accurate quantification of teleconnection impacts is limited, particularly in regards to the ocean and the cryosphere. For example, it is unknown how teleconnection and corresponding atmosphere–ice–ocean interactions influence oceanic heat content[2,3,34,150,151]; how anthropogenic changes in the mean Antarctic state modify the impact of teleconnected signals[24,120,229]; whether tropical–polar teleconnections will influence Antarctic tipping points[246,247]; broader impacts on ecosystems[13,14]; and the relative importance of different ocean basins[56,58]. Solving these questions requires better understanding of the detailed processes and dynamics of the teleconnections, and depends critically on long-lasting observations and continued development of Earth system models.

Third, much of the research to date has focused on West Antarctica, given its strong connections to the ASL, ENSO, the IPO and the AMO. However, many East Antarctic basins are also at risk of anthropogenic climate change[248–250], as exemplified by the Totten Ice Shelf[177].

More research is needed to investigate the potential effects of tropical–polar teleconnections on climate variability over East Antarctica[251,252], particularly from the perspective of the IPO and AMO phase changes in the coming decades. Moreover, in addition to the ASL, two other low-pressure centres of the SAM also contribute to variability in East Antarctic climate, linking to the tropics through additional pathways. These require further investigation based on new observations and numerical model experiments.

Finally, to date, most work has examined teleconnections from the tropics to Antarctica. Variability at high latitudes can also feed back to, or interact with, climate conditions at lower latitudes. For example, changes in SST and sea ice can alter the mean circulation in the tropics[253–255]. While such influences are being increasingly investigated from the Arctic[256–258], efforts are needed to address similar relationships from the Antarctic. In particular, what mechanisms allow changes in the Antarctic to feed back to the tropical and mid-latitude climate; how does the Antarctic interact with lower latitudes; and how much does the Antarctic contribute to the Earth's climate system through these interactions? Ultimately, progress in addressing such important scientific issues will depend critically on sustained global ocean and climate observations, climate model developments and a more comprehensive pan-Antarctic approach.

Published online: 31 August 2021

1. Domingues, C. M. et al. Improved estimates of upper-ocean warming and multi-decadal sea-level rise. *Nature* **453**, 1090–1093 (2008).
2. Gille, S. T. Decadal-scale temperature trends in the Southern Hemisphere ocean. *J. Clim.* **21**, 4749–4765 (2008).
3. Spence, P. et al. Rapid subsurface warming and circulation changes of Antarctic coastal waters by poleward shifting winds. *Geophys. Res. Lett.* **41**, 4601–4610 (2014).
4. Bromwich, D. H. et al. Central West Antarctica among the most rapidly warming regions on Earth. *Nat. Geosci.* **6**, 139–145 (2013).
5. Steig, E. J. et al. Warming of the Antarctic ice-sheet surface since the 1957 International Geophysical Year. *Nature* **457**, 459–462 (2009).
6. Paolo, F. S., Fricker, H. A. & Padman, L. Volume loss from Antarctic ice shelves is accelerating. *Science* **348**, 327–331 (2015).
7. Rignot, E. et al. Recent Antarctic ice mass loss from radar interferometry and regional climate modelling. *Nat. Geosci.* **1**, 106–110 (2008).
8. Meehl, G. A. et al. Sustained ocean changes contributed to sudden Antarctic sea ice retreat in late 2016. *Nat. Commun.* **10**, 14 (2019).
9. Parkinson, C. L. A 40-y record reveals gradual Antarctic sea ice increases followed by decreases at rates far exceeding the rates seen in the Arctic. *Proc. Natl Acad. Sci. USA* **116**, 14414–14423 (2019).
10. Stammerjohn, S. E., Martinson, D. G., Smith, R. C., Yuan, X. & Rind, D. Trends in Antarctic annual sea ice retreat and advance and their relation to El Niño–Southern Oscillation and Southern Annular Mode variability. *J. Geophys. Res. Oceans* **113**, C03S90 (2008).
11. Stuecker, M. F., Bitz, C. M. & Armour, K. C. Conditions leading to the unprecedented low Antarctic sea ice extent during the 2016 austral spring season. *Geophys. Res. Lett.* **44**, 9008–9019 (2017).
12. Turner, J. et al. Unprecedented springtime retreat of Antarctic sea ice in 2016. *Geophys. Res. Lett.* **44**, 6868–6875 (2017).
13. Kennicutt, M. C. II et al. Sustained Antarctic research: a 21st century imperative. *One Earth* **1**, 95–113 (2019).
14. Kennicutt, M. C. et al. A roadmap for Antarctic and Southern Ocean science for the next two decades and beyond. *Antarctic Sci.* **27**, 3–18 (2015).
15. Dutrieux, P. et al. Strong sensitivity of Pine Island ice-shelf melting to climatic variability. *Science* **343**, 174–178 (2014).
16. Joughin, I. & Alley, R. B. Stability of the West Antarctic ice sheet in a warming world. *Nat. Geosci.* **4**, 506–513 (2011).
17. Anilkumar, N., Chacko, R., Sabu, P. & George, J. V. Freshening of Antarctic Bottom Water in the Indian ocean sector of Southern ocean. *Deep. Sea Res. Part II Top. Stud. Oceanogr.* **118**, 162–169 (2015).
18. Haumann, F. A., Gruber, N., Münnich, M., Frenger, I. & Kern, S. Sea-ice transport driving Southern Ocean salinity and its recent trends. *Nature* **537**, 89–92 (2016).
19. Ohshima, K. I. et al. Antarctic Bottom Water production by intense sea-ice formation in the Cape Darnley polynya. *Nat. Geosci.* **6**, 235–240 (2013).
20. Wang, G. et al. Compounding tropical and stratospheric forcing of the record low Antarctic sea-ice in 2016. *Nat. Commun.* **10**, 13 (2019).
21. Jones, M. E. et al. Sixty years of widespread warming in the southern middle and high latitudes (1957–2016). *J. Clim.* **32**, 6875–6898 (2019).
22. Thompson, D. W. & Solomon, S. Interpretation of recent Southern Hemisphere climate change. *Science* **296**, 895–899 (2002).
23. Thompson, D. W. et al. Signatures of the Antarctic ozone hole in Southern Hemisphere surface climate change. *Nat. Geosci.* **4**, 741–749 (2011).
24. Wang, G., Cai, W. & Purich, A. Trends in Southern Hemisphere wind-driven circulation in CMIP5 models over the 21st century: Ozone recovery versus greenhouse forcing. *J. Geophys. Res. Oceans* **119**, 2974–2986 (2014).
25. Arblaster, J. M. & Meehl, G. A. Contributions of external forcings to southern annular mode trends. *J. Clim.* **19**, 2896–2905 (2006).
26. Lecomte, O. et al. Vertical ocean heat redistribution sustaining sea-ice concentration trends in the Ross Sea. *Nat. Commun.* **8**, 258 (2017).
27. Zhang, L., Delworth, T. L., Cooke, W. & Yang, X. Natural variability of Southern Ocean convection as a driver of observed climate trends. *Nat. Clim. Change* **9**, 59–65 (2019).
28. Li, X., Holland, D. M., Gerber, E. P. & Yoo, C. Impacts of the north and tropical Atlantic Ocean on the Antarctic Peninsula and sea ice. *Nature* **505**, 538–542 (2014).
29. Shepherd, A. et al. Mass balance of the antarctic ice sheet from 1992 to 2017. *Nature* **558**, 219–222 (2018).
30. Cavalieri, D. J., Parkinson, C. L. & Vinnikov, K. Y. 30-Year satellite record reveals contrasting Arctic and Antarctic decadal sea ice variability. *Geophys. Res. Lett.* **30**, 1970 (2003).
31. King, J. Climate science: A resolution of the Antarctic paradox. *Nature* **505**, 491–492 (2014).
32. Simpkins, G. R., Ciasto, L. M. & England, M. H. Observed variations in multidecadal Antarctic sea ice trends during 1979–2012. *Geophys. Res. Lett.* **40**, 3643–3648 (2013).
33. Bamber, J. L., Westaway, R. M., Marzeion, B. & Wouters, B. The land ice contribution to sea level during the satellite era. *Environ. Res. Lett.* **13**, 063008 (2018).
34. Schmidtko, S., Heywood, K. J., Thompson, A. F. & Aoki, S. Multidecadal warming of Antarctic waters. *Science* **346**, 1227–1231 (2014).
35. Smith, B. et al. Pervasive ice sheet mass loss reflects competing ocean and atmosphere processes. *Science* **368**, 1239–1242 (2020).
36. Turner, J., Phillips, T., Hosking, J. S., Marshall, G. J. & Orr, A. The Amundsen Sea low. *Int. J. Climatol.* **33**, 1818–1829 (2013).
37. Ding, Q., Steig, E. J., Battisti, D. S. & Küttel, M. Winter warming in West Antarctica caused by central tropical Pacific warming. *Nat. Geosci.* **4**, 398–403 (2011).
38. Meehl, G. A., Hu, A., Santer, B. D. & Xie, S.-P. Contribution of the Interdecadal Pacific Oscillation to twentieth-century global surface temperature trends. *Nat. Clim. Change* **6**, 1005–1008 (2016).
39. Raphael, M. et al. The Amundsen Sea low: Variability, change, and impact on Antarctic climate. *Bull. Am. Meteorol. Soc.* **97**, 111–121 (2016).
40. Ding, Q., Steig, E. J., Battisti, D. S. & Wallace, J. M. Influence of the tropics on the Southern Annular Mode. *J. Clim.* **25**, 6330–6348 (2012).
41. Fogt, R. L. & Bromwich, D. H. Decadal variability of the ENSO teleconnection to the high-latitude South Pacific governed by coupling with the southern annular mode. *J. Clim.* **19**, 979–997 (2006).
42. Fogt, R. L., Bromwich, D. H. & Hines, K. M. Understanding the SAM influence on the South Pacific ENSO teleconnection. *Clim. Dyn.* **36**, 1555–1576 (2011).
43. Hoskins, B. J. & Ambrizzi, T. Rossby wave propagation on a realistic longitudinally varying flow. *J. Atmos. Sci.* **50**, 1661–1671 (1993).
44. Hoskins, B. J. & Karoly, D. J. The steady linear response of a spherical atmosphere to thermal and orographic forcing. *J. Atmos. Sci.* **38**, 1179–1196 (1981).
45. L'Heureux, M. L. & Thompson, D. W. Observed relationships between the El Niño–Southern Oscillation and the extratropical zonal-mean circulation. *J. Clim.* **19**, 276–287 (2006).
46. Schneider, D. P., Deser, C. & Okumura, Y. An assessment and interpretation of the observed warming of West Antarctica in the austral spring. *Clim. Dyn.* **38**, 323–347 (2012).
47. Meehl, G. A., Arblaster, J. M., Bitz, C. M., Chung, C. T. & Teng, H. Antarctic sea-ice expansion between 2000 and 2014 driven by tropical Pacific decadal climate variability. *Nat. Geosci.* **9**, 590–595 (2016).
48. Lefebvre, W., Goosse, H., Timmermann, R. & Fichefet, T. Influence of the Southern Annular Mode on the sea ice–ocean system. *J. Geophys. Res. Oceans* **109**, C09005 (2004).
49. White, W. B. & Peterson, R. G. An Antarctic circumpolar wave in surface pressure, wind, temperature and sea-ice extent. *Nature* **380**, 699–702 (1996).
50. Ding, M. et al. Towards more snow days in summer since 2001 at the Great Wall Station, Antarctic Peninsula: The role of the Amundsen Sea low. *Adv. Atmos. Sci.* **37**, 494–504 (2020).
51. Welhouse, L. J., Lazzara, M. A., Keller, L. M., Tripoli, G. J. & Hitchman, M. H. Composite analysis of the effects of ENSO events on Antarctica. *J. Clim.* **29**, 1797–1808 (2016).
52. Yuan, X. & Li, C. Climate modes in southern high latitudes and their impacts on Antarctic sea ice. *J. Geophys. Res. Oceans* **113**, C06S91 (2008).
53. Yuan, X. & Martinson, D. G. The Antarctic dipole and its predictability. *Geophys. Res. Lett.* **28**, 3609–3612 (2001).
54. Cai, W. et al. Pantropical climate interactions. *Science* **363**, eaav4236 (2019).
55. Li, X., Gerber, E. P., Holland, D. M. & Yoo, C. A Rossby wave bridge from the tropical Atlantic to West Antarctica. *J. Clim.* **28**, 2256–2273 (2015).
56. Li, X., Xie, S.-P., Gille, S. T. & Yoo, C. Atlantic-induced pan-tropical climate change over the past three decades. *Nat. Clim. Change* **6**, 275–279 (2016).
57. Nuncio, M. & Yuan, X. The influence of the Indian Ocean dipole on Antarctic sea ice. *J. Clim.* **28**, 2682–2690 (2015).
58. Simpkins, G. R., Peings, Y. & Magnusdottir, G. Pacific influences on tropical Atlantic teleconnections to the Southern Hemisphere high latitudes. *J. Clim.* **29**, 6425–6444 (2016).
59. Li, X., Holland, D. M., Gerber, E. P. & Yoo, C. Rossby waves mediate impacts of tropical oceans on

West Antarctic atmospheric circulation in austral winter. *J. Clim.* **28**, 8151–8164 (2015).
60. Alexander, M. A. et al. The atmospheric bridge: The influence of ENSO teleconnections on air–sea interaction over the global oceans. *J. Clim.* **15**, 2205–2231 (2002).
61. Kidson, J. W. Principal modes of Southern Hemisphere low-frequency variability obtained from NCEP–NCAR reanalyses. *J. Clim.* **12**, 2808–2830 (1999).
62. Mo, K. C. & Higgins, R. W. The Pacific–South American modes and tropical convection during the Southern Hemisphere winter. *Mon. Weather Rev.* **126**, 1581–1596 (1998).
63. Garreaud, R. & Battisti, D. S. Interannual (ENSO) and interdecadal (ENSO-like) variability in the Southern Hemisphere tropospheric circulation. *J. Clim.* **12**, 2113–2123 (1999).
64. Ding, Q. & Steig, E. J. Temperature change on the Antarctic Peninsula linked to the tropical Pacific. *J. Clim.* **26**, 7570–7585 (2013).
65. Simpkins, G. R., McGregor, S., Taschetto, A. S., Ciasto, L. M. & England, M. H. Tropical connections to climatic change in the extratropical Southern Hemisphere: The role of Atlantic SST trends. *J. Clim.* **27**, 4923–4936 (2014).
66. Ciasto, L. M., Simpkins, G. R. & England, M. H. Teleconnections between tropical Pacific SST anomalies and extratropical Southern Hemisphere climate. *J. Clim.* **28**, 56–65 (2015).
67. Wilson, A. B., Bromwich, D. H. & Hines, K. M. Simulating the mutual forcing of anomalous high southern latitude atmospheric circulation by El Niño flavors and the Southern Annular Mode. *J. Clim.* **29**, 2291–2309 (2016).
68. Hitchman, M. H. & Rogal, M. J. ENSO influences on Southern Hemisphere column ozone during the winter to spring transition. *J. Geophys. Res. Atmos.* **115**, D20104 (2010).
69. Jin, D. & Kirtman, B. P. The impact of ENSO periodicity on North Pacific SST variability. *Clim. Dyn.* **34**, 1015–1039 (2010).
70. Schneider, D. P., Okumura, Y. & Deser, C. Observed Antarctic interannual climate variability and tropical linkages. *J. Clim.* **25**, 4048–4066 (2012).
71. Scott Yiu, Y. Y. & Maycock, A. C. On the seasonality of the El Niño teleconnection to the Amundsen Sea region. *J. Clim.* **32**, 4829–4845 (2019).
72. Karoly, D. J. Southern hemisphere circulation features associated with El Niño-Southern Oscillation events. *J. Clim.* **2**, 1239–1252 (1989).
73. Yuan, X. ENSO-related impacts on Antarctic sea ice: a synthesis of phenomenon and mechanisms. *Antarctic Sci.* **16**, 415–425 (2004).
74. Yuan, X., Kaplan, M. R. & Cane, M. A. The interconnected global climate system — A review of tropical–polar teleconnections. *J. Clim.* **31**, 5765–5792 (2018).
75. Liu, J., Yuan, X., Rind, D. & Martinson, D. G. Mechanism study of the ENSO and southern high latitude climate teleconnections. *Geophys. Res. Lett.* **29**, 24-1–24-4 (2002).
76. Rind, D. et al. Effects of glacial meltwater in the GISS coupled atmosphereocean model: 1. North Atlantic Deep Water response. *J. Geophys. Res. Atmos.* **106**, 27335–27353 (2001).
77. Bals-Elsholz, T. M. et al. The wintertime Southern Hemisphere split jet: Structure, variability, and evolution. *J. Clim.* **14**, 4191–4215 (2001).
78. Chen, B., Smith, S. R. & Bromwich, D. H. Evolution of the tropospheric split jet over the South Pacific Ocean during the 1986–89 ENSO cycle. *Mon. Weather Rev.* **124**, 1711–1731 (1996).
79. Carleton, A. M. & Carpenter, D. A. Satellite climatology of 'polar lows' and broadscale climatic associations for the Southern Hemisphere. *Int. J. Climatol.* **10**, 219–246 (1990).
80. Sinclair, M. R. Objective identification of cyclones and their circulation intensity, and climatology. *Weather Forecast.* **12**, 595–612 (1997).
81. Okumura, Y. M., Schneider, D., Deser, C. & Wilson, R. Decadal–interdecadal climate variability over Antarctica and linkages to the tropics: Analysis of ice core, instrumental, and tropical proxy data. *J. Clim.* **25**, 7421–7441 (2012).
82. Cai, W., Van Rensch, P., Cowan, T. & Hendon, H. H. Teleconnection pathways of ENSO and the IOD and the mechanisms for impacts on Australian rainfall. *J. Clim.* **24**, 3910–3923 (2011).
83. Saji, N., Ambrizzi, T. & Ferraz, S. E. T. Indian Ocean Dipole mode events and austral surface air temperature anomalies. *Dyn. Atmos. Ocean.* **39**, 87–101 (2005).
84. Cai, W. et al. Increased frequency of extreme Indian Ocean Dipole events due to greenhouse warming. *Nature* **510**, 254–258 (2014).
85. Pohl, B., Fauchereau, N., Reason, C. & Rouault, M. Relationships between the Antarctic Oscillation, the Madden–Julian oscillation, and ENSO, and consequences for rainfall analysis. *J. Clim.* **23**, 238–254 (2010).
86. Rondanelli, R., Hatchett, B., Rutllant, J., Bozkurt, D. & Garreaud, R. Strongest MJO on record triggers extreme Atacama rainfall and warmth in Antarctica. *Geophys. Res. Lett.* **46**, 3482–3491 (2019).
87. Yoo, C., Lee, S. & Feldstein, S. The impact of the Madden-Julian oscillation trend on the Antarctic warming during the 1979–2008 austral winter. *Atmos. Sci. Lett.* **13**, 194–199 (2012).
88. Flatau, M. & Kim, Y.-J. Interaction between the MJO and polar circulations. *J. Clim.* **26**, 3562–3574 (2013).
89. Rutllant, J. & Fuenzalida, H. Synoptic aspects of the central Chile rainfall variability associated with the Southern Oscillation. *Int. J. Climatol.* **11**, 63–76 (1991).
90. Pope, J. O., Holland, P. R., Orr, A., Marshall, G. J. & Phillips, T. The impacts of El Niño on the observed sea ice budget of West Antarctica. *Geophys. Res. Lett.* **44**, 6200–6208 (2017).
91. Paolo, F. et al. Response of Pacific-sector Antarctic ice shelves to the El Niño/Southern oscillation. *Nat. Geosci.* **11**, 121–126 (2018).
92. Steig, E. J., Ding, Q., Battisti, D. & Jenkins, A. Tropical forcing of Circumpolar Deep Water inflow and outlet glacier thinning in the Amundsen Sea Embayment, West Antarctica. *Ann. Glaciol.* **53**, 19–28 (2012).
93. Hobbs, W. R. et al. A review of recent changes in Southern Ocean sea ice, their drivers and forcings. *Glob. Planet. Change* **143**, 228–250 (2016).
94. Raphael, M. N. & Hobbs, W. The influence of the large-scale atmospheric circulation on Antarctic sea ice during ice advance and retreat seasons. *Geophys. Res. Lett.* **41**, 5037–5045 (2014).
95. Fogt, R. L. & Zbacnik, E. A. Sensitivity of the Amundsen Sea low to stratospheric ozone depletion. *J. Clim.* **27**, 9383–9400 (2014).
96. Jones, J. M. et al. Assessing recent trends in high-latitude Southern Hemisphere surface climate. *Nat. Clim. Change* **6**, 917–926 (2016).
97. Turner, J. et al. Non-annular atmospheric circulation change induced by stratospheric ozone depletion and its role in the recent increase of Antarctic sea ice extent. *Geophys. Res. Lett.* **36**, L08502 (2009).
98. Henley, B. J. et al. A tripole index for the interdecadal Pacific oscillation. *Clim. Dyn.* **45**, 3077–3090 (2015).
99. Purich, A., Cai, W., England, M. H. & Cowan, T. Evidence for link between modelled trends in Antarctic sea ice and underestimated westerly wind changes. *Nat. Commun.* **7**, 10409 (2016).
100. Meehl, G. A., Hu, A. & Teng, H. Initialized decadal prediction for transition to positive phase of the Interdecadal Pacific Oscillation. *Nat. Commun.* **7**, 11718 (2016).
101. Clem, K. R. & Fogt, R. L. South Pacific circulation changes and their connection to the tropics and regional Antarctic warming in austral spring, 1979–2012. *J. Geophys. Res. Atmos.* **120**, 2773–2792 (2015).
102. Brown, J. R. et al. South Pacific Convergence Zone dynamics, variability and impacts in a changing climate. *Nat. Rev. Earth Environ.* **1**, 530–543 (2020).
103. Clem, K. R., Lintner, B. R., Broccoli, A. J. & Miller, J. R. Role of the South Pacific convergence zone in West Antarctic decadal climate variability. *Geophys. Res. Lett.* **46**, 6900–6909 (2019).
104. Clem, K. R., Renwick, J. A., McGregor, J. & Fogt, R. L. The relative influence of ENSO and SAM on Antarctic Peninsula climate. *J. Geophys. Res. Atmos.* **121**, 9324–9341 (2016).
105. Schlesinger, M. E. & Ramankutty, N. An oscillation in the global climate system of period 65–70 years. *Nature* **367**, 723–726 (1994).
106. McGregor, S. et al. Recent Walker circulation strengthening and Pacific cooling amplified by Atlantic warming. *Nat. Clim. Change* **4**, 888–892 (2014).
107. Meehl, G. A. et al. Atlantic and Pacific tropics connected by mutually interactive decadal-timescale processes. *Nat. Geosci.* **14**, 36–42 (2021).
108. Marshall, G. J., Di Battista, S., Naik, S. S. & Thamban, M. Analysis of a regional change in the sign of the SAM–temperature relationship in Antarctica. *Clim. Dyn.* **36**, 277–287 (2011).
109. Nicolas, J. P. & Bromwich, D. H. New reconstruction of Antarctic near-surface temperatures: Multidecadal trends and reliability of global reanalyses. *J. Clim.* **27**, 8070–8093 (2014).
110. Bromwich, D. H. et al. Tropospheric clouds in Antarctica. *Rev. Geophys.* **50**, RG1004 (2012).
111. Wang, Y., Huang, G. & Hu, K. Internal variability in multidecadal trends of surface air temperature over Antarctica in austral winter in model simulations. *Clim. Dyn.* **55**, 2835–2847 (2020).
112. Turner, J. et al. Absence of 21st century warming on Antarctic Peninsula consistent with natural variability. *Nature* **535**, 411–415 (2016).
113. Clem, K. R. et al. Record warming at the South Pole during the past three decades. *Nat. Clim. Change* **10**, 762–770 (2020).
114. Kwok, R., Comiso, J. C., Lee, T. & Holland, P. R. Linked trends in the South Pacific sea ice edge and Southern Oscillation Index. *Geophys. Res. Lett.* **43**, 10,295–10,302 (2016).
115. Schneider, D. P. & Deser, C. Tropically driven and externally forced patterns of Antarctic sea ice change: Reconciling observed and modeled trends. *Clim. Dyn.* **50**, 4599–4618 (2018).
116. Turner, J. et al. Antarctic Temperature Variability and Change from Station Data. *Int. J. Climatol.* **40**, 2986–3007 (2020).
117. Orr, A. et al. Characteristics of summer airflow over the Antarctic Peninsula in response to recent strengthening of westerly circumpolar winds. *J. Atmos. Sci.* **65**, 1396–1413 (2008).
118. Van Lipzig, N. P., Marshall, G. J., Orr, A. & King, J. C. The relationship between the Southern Hemisphere Annular Mode and Antarctic Peninsula summer temperatures: Analysis of a high-resolution model climatology. *J. Clim.* **21**, 1649–1668 (2008).
119. Holland, P. R. The seasonality of Antarctic sea ice trends. *Geophys. Res. Lett.* **41**, 4230–4237 (2014).
120. Lu, J., Vecchi, G. A. & Reichler, T. Expansion of the Hadley cell under global warming. *Geophys. Res. Lett.* **34**, L06805 (2007).
121. Meehl, G. A., Chung, C. T. Y., Arblaster, J. M., Holland, M. M. & Bitz, C. M. Tropical decadal variability and the rate of Arctic sea ice decrease. *Geophys. Res. Lett.* **45**, 11,326–11,333 (2018).
122. Stammerjohn, S., Massom, R., Rind, D. & Martinson, D. Regions of rapid sea ice change: An inter-hemispheric seasonal comparison. *Geophys. Res. Lett.* **39**, L06501 (2012).
123. Jacobs, S. S. & Comiso, J. C. Climate variability in the Amundsen and Bellingshausen Seas. *J. Clim.* **10**, 697–709 (1997).
124. Liu, Z. & Wu, L. Atmospheric response to North Pacific SST: the role of ocean–atmosphere coupling. *J. Clim.* **17**, 1859–1882 (2004).
125. Smith, R. C. & Stammerjohn, S. E. Variations of surface air temperature and sea-ice extent in the western Antarctic Peninsula region. *Ann. Glaciol.* **33**, 493–500 (2001).
126. Yuan, X. & Martinson, D. G. Antarctic sea ice extent variability and its global connectivity. *J. Clim.* **13**, 1697–1717 (2000).
127. Parkinson, C. L. Southern Ocean sea ice and its wider linkages: insights revealed from models and observations. *Antarctic Sci.* **16**, 387–400 (2004).
128. Stammerjohn, S. & Smith, R. Opposing Southern Ocean climate patterns as revealed by trends in regional sea ice coverage. *Clim. Change* **37**, 617–639 (1997).
129. Holland, M. M., Landrum, L., Raphael, M. N. & Kwok, R. The regional, seasonal, and lagged influence of the Amundsen sea low on Antarctic sea ice. *Geophys. Res. Lett.* **45**, 11227–11234 (2018).
130. Holland, P. R. & Kwok, R. Wind-driven trends in Antarctic sea-ice drift. *Nat. Geosci.* **5**, 872–875 (2012).
131. Hosking, J. S., Orr, A., Marshall, G. J., Turner, J. & Phillips, T. The influence of the Amundsen–Bellingshausen Seas low on the climate of West Antarctica and its representation in coupled climate model simulations. *J. Clim.* **26**, 6633–6648 (2013).
132. Haumann, F. A., Notz, D. & Schmidt, H. Anthropogenic influence on recent circulation-driven Antarctic sea ice changes. *Geophys. Res. Lett.* **41**, 8429–8437 (2014).
133. Kwok, R., Pang, S. S., Kacimi, S. & Carmack, E. C. Sea ice drift in the Southern Ocean: Regional patterns, variability, and trends. *Elementa Sci. Anthrop.* **5**, 32 (2017).
134. Raphael, M. N. & Holland, M. M. Twentieth century simulation of the Southern Hemisphere climate in coupled models. Part 1: Large scale circulation variability. *Clim. Dyn.* **26**, 217–228 (2006).
135. Turner, J. et al. Atmosphere-ocean-ice interactions in the Amundsen Sea embayment, West Antarctica. *Rev. Geophys.* **55**, 235–276 (2017).

136. Goosse, H. & Zunz, V. Decadal trends in the Antarctic sea ice extent ultimately controlled by ice–ocean feedback. *Cryosphere* **8**, 453–470 (2014).
137. Bintanja, R., Van Oldenborgh, G., Drijfhout, S., Wouters, B. & Katsman, C. Important role for ocean warming and increased ice-shelf melt in Antarctic sea-ice expansion. *Nat. Geosci.* **6**, 376–379 (2013).
138. Haumann, F. A., Gruber, N. & Münnich, M. Sea-ice induced Southern Ocean subsurface warming and surface cooling in a warming climate. *AGU Adv.* **1**, e2019AV000132 (2020).
139. Schlosser, E., Haumann, F. A. & Raphael, M. N. Atmospheric influences on the anomalous 2016 Antarctic sea ice decay. *Cryosphere* **12**, 1103–1119 (2018).
140. Wang, Z., Turner, J., Wu, Y. & Liu, C. Rapid decline of total antarctic sea ice extent during 2014–16 controlled by wind-driven sea ice drift. *J. Clim.* **32**, 5381–5395 (2019).
141. Purich, A. & England, M. H. Tropical teleconnections to Antarctic sea ice during austral spring 2016 in coupled pacemaker experiments. *Geophys. Res. Lett.* **46**, 6848–6858 (2019).
142. Hu, S. & Fedorov, A. V. The extreme El Niño of 2015–2016 and the end of global warming hiatus. *Geophys. Res. Lett.* **44**, 3816–3824 (2017).
143. Thoma, M., Greatbatch, R. J., Kadow, C. & Gerdes, R. Decadal hindcasts initialized using observed surface wind stress: Evaluation and prediction out to 2024. *Geophys. Res. Lett.* **42**, 6454–6461 (2015).
144. Armour, K. C., Marshall, J., Scott, J. R., Donohoe, A. & Newsom, E. R. Southern Ocean warming delayed by circumpolar upwelling and equatorward transport. *Nat. Geosci.* **9**, 549–554 (2016).
145. Böning, C. W., Dispert, A., Visbeck, M., Rintoul, S. & Schwarzkopf, F. U. The response of the Antarctic Circumpolar Current to recent climate change. *Nat. Geosci.* **1**, 864–869 (2008).
146. Giglio, D. & Johnson, G. C. Middepth decadal warming and freshening in the South Atlantic. *J. Geophys. Res. Oceans* **122**, 973–979 (2017).
147. Gille, S. T. Warming of the Southern Ocean since the 1950s. *Science* **295**, 1275–1277 (2002).
148. Purkey, S. G. & Johnson, G. C. Warming of global abyssal and deep Southern Ocean waters between the 1990s and 2000s: Contributions to global heat and sea level rise budgets. *J. Clim.* **23**, 6336–6351 (2010).
149. Talley, L. et al. Changes in ocean heat, carbon content, and ventilation: a review of the first decade of GO-SHIP global repeat hydrography. *Annu. Rev. Mar. Sci.* **8**, 185–215 (2016).
150. Cazenave, A. & Llovel, W. Contemporary sea level rise. *Annu. Rev. Mar. Sci.* **2**, 145–173 (2010).
151. Stammer, D., Cazenave, A., Ponte, R. M. & Tamisiea, M. E. Causes for contemporary regional sea level changes. *Annu. Rev. Mar. Sci.* **5**, 21–46 (2013).
152. Swart, N. C., Gille, S. T., Fyfe, J. C. & Gillett, N. P. Recent Southern Ocean warming and freshening driven by greenhouse gas emissions and ozone depletion. *Nat. Geosci.* **11**, 836–841 (2018).
153. Cai, W., Cowan, T., Godfrey, S. & Wijffels, S. Simulations of processes associated with the fast warming rate of the southern midlatitude ocean. *J. Clim.* **23**, 197–206 (2010).
154. Fan, T., Deser, C. & Schneider, D. P. Recent Antarctic sea ice trends in the context of Southern Ocean surface climate variations since 1950. *Geophys. Res. Lett.* **41**, 2419–2426 (2014).
155. Meredith, M. P. & King, J. C. Rapid climate change in the ocean west of the Antarctic Peninsula during the second half of the 20th century. *Geophys. Res. Lett.* **32**, L19604 (2005).
156. Cook, A. J. et al. Ocean forcing of glacier retreat in the western Antarctic Peninsula. *Science* **353**, 283–286 (2016).
157. Martinson, D. G., Stammerjohn, S. E., Iannuzzi, R. A., Smith, R. C. & Vernet, M. Western Antarctic Peninsula physical oceanography and spatio–temporal variability. *Deep. Sea Res. Part II Top. Stud. Oceanogr.* **55**, 1964–1987 (2008).
158. Spence, P. et al. Localized rapid warming of West Antarctic subsurface waters by remote winds. *Nat. Clim. Change* **7**, 595–603 (2017).
159. Holland, P. R., Bracegirdle, T. J., Dutrieux, P., Jenkins, A. & Steig, E. J. West Antarctic ice loss influenced by internal climate variability and anthropogenic forcing. *Nat. Geosci.* **12**, 718–724 (2019).
160. Jenkins, A. et al. West Antarctic Ice Sheet retreat in the Amundsen Sea driven by decadal oceanic variability. *Nat. Geosci.* **11**, 733–738 (2018).
161. Thoma, M., Jenkins, A., Holland, D. & Jacobs, S. Modelling circumpolar deep water intrusions on the Amundsen Sea continental shelf, Antarctica. *Geophys. Res. Lett.* **35**, L18602 (2008).
162. Auger, M., Morrow, R., Kestenare, E., Sallée, J.-B. & Cowley, R. Southern Ocean in-situ temperature trends over 25 years emerge from interannual variability. *Nat. Commun.* **12**, 514 (2021).
163. Hellmer, H. H., Kauker, F., Timmermann, R., Determann, J. & Rae, J. Twenty-first-century warming of a large Antarctic ice-shelf cavity by a redirected coastal current. *Nature* **485**, 225–228 (2012).
164. Jacobs, S. et al. The Amundsen Sea and the Antarctic ice sheet. *Oceanography* **25**, 154–163 (2012).
165. Durack, P. J., Wijffels, S. E. & Matear, R. J. Ocean salinities reveal strong global water cycle intensification during 1950 to 2000. *Science* **336**, 455–458 (2012).
166. Helm, K. P., Bindoff, N. L. & Church, J. A. Changes in the global hydrological-cycle inferred from ocean salinity. *Geophys. Res. Lett.* **37**, L18701 (2010).
167. Purkey, S. G. & Johnson, G. C. Antarctic Bottom Water warming and freshening: Contributions to sea level rise, ocean freshwater budgets, and global heat gain. *J. Clim.* **26**, 6105–6122 (2013).
168. van Wijk, E. M. & Rintoul, S. R. Freshening drives contraction of Antarctic bottom water in the Australian Antarctic Basin. *Geophys. Res. Lett.* **41**, 1657–1664 (2014).
169. Swart, N. & Fyfe, J. The influence of recent Antarctic ice sheet retreat on simulated sea ice area trends. *Geophys. Res. Lett.* **40**, 4328–4332 (2013).
170. Dotto, T. S. et al. Variability of the Ross Gyre, Southern Ocean: drivers and responses revealed by satellite altimetry. *Geophys. Res. Lett.* **45**, 6195–6204 (2018).
171. Meijers, A., Cerovečki, I., King, B. A. & Tamsitt, V. A see-saw in Pacific subantarctic mode water formation driven by atmospheric modes. *Geophys. Res. Lett.* **46**, 13152–13160 (2019).
172. Pritchard, H. et al. Antarctic ice-sheet loss driven by basal melting of ice shelves. *Nature* **484**, 502–505 (2012).
173. Rignot, E. et al. Four decades of Antarctic Ice Sheet mass balance from 1979–2017. *Proc. Natl Acad. Sci. USA* **116**, 1095–1103 (2019).
174. Shepherd, A. et al. Trends in Antarctic Ice Sheet elevation and mass. *Geophys. Res. Lett.* **46**, 8174–8183 (2019).
175. Scott, R. C., Nicolas, J. P., Bromwich, D. H., Norris, J. R. & Lubin, D. Meteorological drivers and large-scale climate forcing of West Antarctic surface melt. *J. Clim.* **32**, 665–684 (2019).
176. Wouters, B. et al. Dynamic thinning of glaciers on the Southern Antarctic Peninsula. *Science* **348**, 899–903 (2015).
177. Mohajerani, Y., Velicogna, I. & Rignot, E. Mass loss of Totten and Moscow University glaciers, East Antarctica, using regionally optimized GRACE mascons. *Geophys. Res. Lett.* **45**, 7010–7018 (2018).
178. Jenkins, A. et al. Decadal ocean forcing and Antarctic ice sheet response: Lessons from the Amundsen Sea. *Oceanography* **29**, 106–117 (2016).
179. Gudmundsson, G. H., Paolo, F. S., Adusumilli, S. & Fricker, H. A. Instantaneous Antarctic ice sheet mass loss driven by thinning ice shelves. *Geophys. Res. Lett.* **46**, 13903–13909 (2019).
180. Joughin, I., Smith, B. E. & Medley, B. Marine ice sheet collapse potentially under way for the Thwaites Glacier Basin, West Antarctica. *Science* **344**, 735–738 (2014).
181. Mouginot, J., Rignot, E. & Scheuchl, B. Sustained increase in ice discharge from the Amundsen Sea Embayment, West Antarctica, from 1973 to 2013. *Geophys. Res. Lett.* **41**, 1576–1584 (2014).
182. Seroussi, H. et al. Continued retreat of Thwaites Glacier, West Antarctica, controlled by bed topography and ocean circulation. *Geophys. Res. Lett.* **44**, 6191–6199 (2017).
183. Davis, P. E. et al. Variability in basal melting beneath Pine Island Ice Shelf on weekly to monthly timescales. *J. Geophys. Res. Oceans* **123**, 8655–8669 (2018).
184. Kimura, S. et al. Oceanographic controls on the variability of ice-shelf basal melting and circulation of glacial meltwater in the Amundsen Sea Embayment, Antarctica. *J. Geophys. Res. Oceans* **122**, 10131–10155 (2017).
185. Berthier, E., Scambos, T. A. & Shuman, C. A. Mass loss of Larsen B tributary glaciers (Antarctic Peninsula) unabated since 2002. *Geophys. Res. Lett.* **39**, L13501 (2012).
186. Minchew, B. M., Gudmundsson, G. H., Gardner, A. S., Paolo, F. S. & Fricker, H. A. Modeling the dynamic response of outlet glaciers to observed ice-shelf thinning in the Bellingshausen Sea Sector, West Antarctica. *J. Glaciol.* **64**, 333–342 (2018).
187. Royston, S. & Gudmundsson, G. H. Changes in ice-shelf buttressing following the collapse of Larsen A Ice Shelf, Antarctica, and the resulting impact on tributaries. *J. Glaciol.* **62**, 905–911 (2016).
188. Scambos, T. A., Hulbe, C., Fahnestock, M. & Bohlander, J. The link between climate warming and break-up of ice shelves in the Antarctic Peninsula. *J. Glaciol.* **46**, 516–530 (2000).
189. Barrand, N. et al. Trends in Antarctic Peninsula surface melting conditions from observations and regional climate modeling. *J. Geophys. Res. Earth Surf.* **118**, 315–330 (2013).
190. Massom, R. A. et al. Antarctic ice shelf disintegration triggered by sea ice loss and ocean swell. *Nature* **558**, 383–389 (2018).
191. Bronselaer, B. et al. Change in future climate due to Antarctic meltwater. *Nature* **564**, 53–58 (2018).
192. Hunke, E. C. & Comeau, D. Sea ice and iceberg dynamic interaction. *J. Geophys. Res. Oceans* **116**, C05008 (2011).
193. Jeong, H. et al. Impacts of ice-shelf melting on water-mass transformation in the Southern Ocean from E3SM simulations. *J. Clim.* **33**, 5787–5807 (2020).
194. Stern, A., Adcroft, A. & Sergienko, O. The effects of Antarctic iceberg calving-size distribution in a global climate model. *J. Geophys. Res. Oceans* **121**, 5773–5788 (2016).
195. Frölicher, T. L. et al. Dominance of the Southern Ocean in anthropogenic carbon and heat uptake in CMIP5 models. *J. Clim.* **28**, 862–886 (2015).
196. Silvano, A. et al. Recent recovery of Antarctic Bottom Water formation in the Ross Sea driven by climate anomalies. *Nat. Geosci.* **13**, 780–786 (2020).
197. Marshall, J. & Speer, K. Closure of the meridional overturning circulation through Southern Ocean upwelling. *Nat. Geosci.* **5**, 171–180 (2012).
198. Landschützer, P. et al. The reinvigoration of the Southern Ocean carbon sink. *Science* **349**, 1221–1224 (2015).
199. Sigman, D. M., Hain, M. P. & Haug, G. H. The polar ocean and glacial cycles in atmospheric CO_2 concentration. *Nature* **466**, 47–55 (2010).
200. Rye, C. D. et al. Rapid sea-level rise along the Antarctic margins in response to increased glacial discharge. *Nat. Geosci.* **7**, 732–735 (2014).
201. Chen, X. & Tung, K.-K. Global surface warming enhanced by weak Atlantic overturning circulation. *Nature* **559**, 387–391 (2018).
202. Roemmich, D. et al. Unabated planetary warming and its ocean structure since 2006. *Nat. Clim. Change* **5**, 240–245 (2015).
203. Chen, X. et al. The increasing rate of global mean sea-level rise during 1993–2014. *Nat. Clim. Change* **7**, 492–495 (2017).
204. Armitage, T. W., Kwok, R., Thompson, A. F. & Cunningham, G. Dynamic topography and sea level anomalies of the Southern Ocean: Variability and teleconnections. *J. Geophys. Res. Oceans* **123**, 613–630 (2018).
205. Cai, W. Antarctic ozone depletion causes an intensification of the Southern Ocean super-gyre circulation. *Geophys. Res. Lett.* **33**, L03712 (2006).
206. Xie, S.-P. et al. Global warming pattern formation: Sea surface temperature and rainfall. *J. Clim.* **23**, 966–986 (2010).
207. Cai, W. et al. ENSO and greenhouse warming. *Nat. Clim. Change* **5**, 849–859 (2015).
208. Cai, W. et al. More extreme swings of the South Pacific convergence zone due to greenhouse warming. *Nature* **488**, 365–369 (2012).
209. Cai, W. et al. Butterfly effect and a self-modulating El Niño response to global warming. *Nature* **585**, 68–73 (2020).
210. Maher, N., Matei, D., Milinski, S. & Marotzke, J. ENSO change in climate projections: Forced response or internal variability? *Geophys. Res. Lett.* **45**, 390–311,398 (2018).
211. Zheng, X.-T., Hui, C. & Yeh, S.-W. Response of ENSO amplitude to global warming in CESM large ensemble: uncertainty due to internal variability. *Clim. Dyn.* **50**, 4019–4035 (2018).
212. Cai, W. et al. Increased variability of eastern Pacific El Niño under greenhouse warming. *Nature* **564**, 201–206 (2018).
213. Jin, F.-F. An equatorial ocean recharge paradigm for ENSO. Part I: Conceptual model. *J. Atmos. Sci.* **54**, 811–829 (1997).
214. Hui, C. & Zheng, X.-T. Uncertainty in Indian Ocean dipole response to global warming: The role of internal variability. *Clim. Dyn.* **51**, 3597–3611 (2018).

215. Zheng, X.-T. et al. Indian Ocean dipole response to global warming in the CMIP5 multimodel ensemble. *J. Clim.* **26**, 6067–6080 (2013).
216. Cai, W. et al. Opposite response of strong and moderate positive Indian Ocean Dipole to global warming. *Nat. Clim. Change* **11**, 27–32 (2021).
217. Cai, W. et al. Climate impacts of the El Niño–Southern Oscillation on South America. *Nat. Rev. Earth Environ.* **1**, 215–231 (2020).
218. Bonfils, C. J. et al. Relative contributions of mean-state shifts and ENSO-driven variability to precipitation changes in a warming climate. *J. Clim.* **28**, 9997–10013 (2015).
219. Chen, Z., Gan, B., Wu, L. & Jia, F. Pacific-North American teleconnection and North Pacific Oscillation: historical simulation and future projection in CMIP5 models. *Clim. Dyn.* **50**, 4379–4403 (2018).
220. Huang, P. Time-varying response of ENSO-induced tropical Pacific rainfall to global warming in CMIP5 models. Part I: Multimodel ensemble results. *J. Clim.* **29**, 5763–5778 (2016).
221. Yan, Z. et al. Eastward shift and extension of ENSO-induced tropical precipitation anomalies under global warming. *Sci. Adv.* **6**, eaax4177 (2020).
222. Yeh, S. W. et al. ENSO atmospheric teleconnections and their response to greenhouse gas forcing. *Rev. Geophys.* **56**, 185–206 (2018).
223. Zhou, Z.-Q., Xie, S.-P., Zheng, X.-T., Liu, Q. & Wang, H. Global warming–induced changes in El Niño teleconnections over the North Pacific and North America. *J. Clim.* **27**, 9050–9064 (2014).
224. Cai, W. et al. Changing El Niño–Southern Oscillation in a warming climate. *Nat. Rev. Earth Environ.* https://doi.org/10.1038/s43017-021-00199-z (2021).
225. Cheng, J. et al. Reduced interdecadal variability of Atlantic Meridional Overturning Circulation under global warming. *Proc. Natl Acad. Sci. USA* **113**, 3175–3178 (2016).
226. Geng, T., Yang, Y. & Wu, L. On the mechanisms of Pacific decadal oscillation modulation in a warming climate. *J. Clim.* **32**, 1443–1459 (2019).
227. Li, S. et al. The Pacific Decadal Oscillation less predictable under greenhouse warming. *Nat. Clim. Change* **10**, 30–34 (2020).
228. Lu, J., Vecchi, G. A. & Reichler, T. Correction to "Expansion of the Hadley cell under global warming". *Geophys. Res. Lett.* **34**, L14808 (2007).
229. Fyfe, J., Boer, G. & Flato, G. The Arctic and Antarctic Oscillations and their projected changes under global warming. *Geophys. Res. Lett.* **26**, 1601–1604 (1999).
230. Fyfe, J. C., Saenko, O. A., Zickfeld, K., Eby, M. & Weaver, A. J. The role of poleward-intensifying winds on Southern Ocean warming. *J. Clim.* **20**, 5391–5400 (2007).
231. Cai, W., Shi, G., Cowan, T., Bi, D. & Ribbe, J. The response of the Southern Annular Mode, the East Australian Current, and the southern mid-latitude ocean circulation to global warming. *Geophys. Res. Lett.* **32**, L23706 (2005).
232. Russell, J. L., Dixon, K. W., Gnanadesikan, A., Stouffer, R. J. & Toggweiler, J. The Southern Hemisphere westerlies in a warming world: Propping open the door to the deep ocean. *J. Clim.* **19**, 6382–6390 (2006).
233. Bracegirdle, T. J. et al. Twenty first century changes in Antarctic and Southern Ocean surface climate in CMIP6. *Atmos. Sci. Lett.* **21**, e984 (2020).
234. Holland, D. M., Nicholls, K. W. & Basinski, A. The Southern Ocean and its interaction with the Antarctic Ice Sheet. *Science* **367**, 1326–1330 (2020).
235. Marzeion, B., Cogley, J. G., Richter, K. & Parkes, D. Attribution of global glacier mass loss to anthropogenic and natural causes. *Science* **345**, 919–921 (2014).
236. McMillan, M. et al. Increased ice losses from Antarctica detected by CryoSat-2. *Geophys. Res. Lett.* **41**, 3899–3905 (2014).
237. Riser, S. C., Swift, D. & Drucker, R. Profiling floats in SOCCOM: Technical capabilities for studying the Southern Ocean. *J. Geophys. Res. Oceans* **123**, 4055–4073 (2018).
238. Zilberman, N. Deep Argo: sampling the total ocean volume in state of the climate in 2016. *Bull. Am. Meteorol. Soc.* **98**, S73–S74 (2017).
239. Lange, B. A., Katlein, C., Nicolaus, M., Peeken, I. & Flores, H. Sea ice algae chlorophyll a concentrations derived from under-ice spectral radiation profiling platforms. *J. Geophys. Res. Oceans* **121**, 8511–8534 (2016).
240. Lazzara, M. A., Weidner, G. A., Keller, L. M., Thom, J. E. & Cassano, J. J. Antarctic automatic weather station program: 30 years of polar observation. *Bull. Am. Meteorol. Soc.* **93**, 1519–1537 (2012).
241. Lai, C.-Y. et al. Vulnerability of Antarctica's ice shelves to meltwater-driven fracture. *Nature* **584**, 574–578 (2020).
242. Hyder, P. et al. Critical Southern Ocean climate model biases traced to atmospheric model cloud errors. *Nat. Commun.* **9**, 3625 (2018).
243. Li, G. & Xie, S.-P. Tropical biases in CMIP5 multimodel ensemble: The excessive equatorial Pacific cold tongue and double ITCZ problems. *J. Clim.* **27**, 1765–1780 (2014).
244. Kosaka, Y. & Xie, S.-P. Recent global-warming hiatus tied to equatorial Pacific surface cooling. *Nature* **501**, 403–407 (2013).
245. Kay, J. E. et al. The Community Earth System Model (CESM) large ensemble project: A community resource for studying climate change in the presence of internal climate variability. *Bull. Am. Meteorol. Soc.* **96**, 1333–1349 (2015).
246. Lenton, T. M. et al. Tipping elements in the Earth's climate system. *Proc. Natl Acad. Sci. USA* **105**, 1786–1793 (2008).
247. Steffen, W. et al. Planetary boundaries: Guiding human development on a changing planet. *Science* **347**, 1259855 (2015).
248. DeConto, R. M. & Pollard, D. Contribution of Antarctica to past and future sea-level rise. *Nature* **531**, 591–597 (2016).
249. Fretwell, P. et al. Bedmap2: improved ice bed, surface and thickness datasets for Antarctica. *Cryosphere* **7**, 375–393 (2013).
250. Morlighem, M. et al. Deep glacial troughs and stabilizing ridges unveiled beneath the margins of the Antarctic ice sheet. *Nat. Geosci.* **13**, 132–137 (2020).
251. Clem, K. R., Renwick, J. A. & McGregor, J. Autumn cooling of Western East Antarctica linked to the tropical Pacific. *J. Geophys. Res. Atmos.* **123**, 89–107 (2018).
252. Marshall, G. J. & Thompson, D. W. The signatures of large-scale patterns of atmospheric variability in Antarctic surface temperatures. *J. Geophys. Res. Atmos.* **121**, 3276–3289 (2016).
253. England, M. R., Polvani, L. M., Sun, L. & Deser, C. Tropical climate responses to projected Arctic and Antarctic sea-ice loss. *Nat. Geosci.* **13**, 275–381 (2020).
254. Hwang, Y. T., Xie, S. P., Deser, C. & Kang, S. M. Connecting tropical climate change with Southern Ocean heat uptake. *Geophys. Res. Lett.* **44**, 9449–9457 (2017).
255. Zhang, X., Deser, C. & Sun, L. Is there a tropical response to recent observed Southern Ocean cooling? *Geophys. Res. Lett.* **48**, e2020GL091235 (2020).
256. Cohen, J. L., Furtado, J. C., Barlow, M. A., Alexeev, V. A. & Cherry, J. E. Arctic warming, increasing snow cover and widespread boreal winter cooling. *Environ. Res. Lett.* **7**, 014007 (2012).
257. Mori, M., Watanabe, M., Shiogama, H., Inoue, J. & Kimoto, M. Robust Arctic sea-ice influence on the frequent Eurasian cold winters in past decades. *Nat. Geosci.* **7**, 869–873 (2014).
258. Zhang, J., Tian, W., Chipperfield, M. P., Xie, F. & Huang, J. Persistent shift of the Arctic polar vortex towards the Eurasian continent in recent decades. *Nat. Clim. Change* **6**, 1094–1099 (2016).
259. Rayner, N. A. et al. Global analyses of sea surface temperature, sea ice, and night marine air temperature since the late nineteenth century. *J. Geophys. Res. Atmos.* **108**, 4407 (2003).
260. Turner, J. et al. The SCAR READER project: Toward a high-quality database of mean Antarctic meteorological observations. *J. Clim.* **17**, 2890–2898 (2004).
261. Peng, G., Meier, W. N., Scott, D. & Savoie, M. A long-term and reproducible passive microwave sea ice concentration data record for climate studies and monitoring. *Earth Syst. Sci. Data* **5**, 311–318 (2013).
262. Good, S. A., Martin, M. J. & Rayner, N. A. EN4: Quality controlled ocean temperature and salinity profiles and monthly objective analyses with uncertainty estimates. *J. Geophys. Res. Oceans* **118**, 6704–6716 (2013).
263. Cheng, L. & Zhu, J. Benefits of CMIP5 multimodel ensemble in reconstructing historical ocean subsurface temperature variations. *J. Clim.* **29**, 5393–5416 (2016).
264. Ishii, M. et al. Accuracy of global upper ocean heat content estimation expected from present observational data sets. *Sola* **13**, 163–167 (2017).
265. Feng, X. et al. A multidecadal-scale tropically driven global teleconnection over the past millennium and its recent strengthening. *J. Clim.* **34**, 2549–2565 (2021).
266. Huang, Y., Ding, Q., Dong, X., Xi, B. & Baxter, I. Summertime low clouds mediate the impact of the large-scale circulation on Arctic sea ice. *Commun. Earth Environ.* **2**, 38 (2021).
267. Trenberth, K. E., Fasullo, J. T., Branstator, G. & Phillips, A. S. Seasonal aspects of the recent pause in surface warming. *Nat. Clim. Change* **4**, 911–916 (2014).
268. Grunseich, G. & Wang, B. Arctic sea ice patterns driven by the Asian summer monsoon. *J. Clim.* **29**, 9097–9112 (2016).
269. Wu, B. & Francis, J. A. Summer Arctic cold anomaly dynamically linked to East Asian heat waves. *J. Clim.* **32**, 1137–1150 (2019).
270. Wu, B., Zhang, R., Wang, B. & D'Arrigo, R. On the association between spring Arctic sea ice concentration and Chinese summer rainfall. *Geophys. Res. Lett.* **36**, L09501 (2009).
271. Labe, Z., Peings, Y. & Magnusdottir, G. The effect of QBO phase on the atmospheric response to projected Arctic sea ice loss in early winter. *Geophys. Res. Lett.* **46**, 7663–7671 (2019).
272. Lee, S., Gong, T., Johnson, N. C., Feldstein, S. B. & Pollard, D. On the possible link between tropical convection and the Northern Hemisphere Arctic surface air temperature change between 1958 and 2001. *J. Clim.* **24**, 4350–4367 (2011).
273. Martin, Z. et al. The influence of the quasi-biennial oscillation on the Madden–Julian oscillation. *Nat. Rev. Earth Environ.* **2**, 477–489 (2021).
274. Steig, E. J. et al. Recent climate and ice-sheet changes in West Antarctica compared with the past 2,000 years. *Nat. Geosci.* **6**, 372–375 (2013).
275. Shakun, J. D. et al. Global warming preceded by increasing carbon dioxide concentrations during the last deglaciation. *Nature* **484**, 49–54 (2012).
276. Tudhope, A. W. et al. Variability in the El Niño-Southern Oscillation through a glacial-interglacial cycle. *Science* **291**, 1511–1517 (2001).
277. Turney, C. S. et al. Millennial and orbital variations of El Nino/Southern Oscillation and high-latitude climate in the last glacial period. *Nature* **428**, 306–310 (2004).
278. Ford, H. L., Ravelo, A. C. & Polissar, P. J. Reduced El Niño–Southern Oscillation during the last glacial maximum. *Science* **347**, 255–258 (2015).
279. Merkel, U., Prange, M. & Schulz, M. ENSO variability and teleconnections during glacial climates. *Quat. Sci. Rev.* **29**, 86–100 (2010).
280. Sadekov, A. Y. et al. Palaeoclimate reconstructions reveal a strong link between El Niño-Southern Oscillation and Tropical Pacific mean state. *Nat. Commun.* **4**, 2692 (2013).
281. Jones, T. R. et al. Southern Hemisphere climate variability forced by Northern Hemisphere ice-sheet topography. *Nature* **554**, 351–355 (2018).
282. Blunier, T. et al. Asynchrony of Antarctic and Greenland climate change during the last glacial period. *Nature* **394**, 739–743 (1998).
283. Dansgaard, W. et al. A new Greenland deep ice core. *Science* **218**, 1273–1277 (1982).
284. Menviel, L. C., Skinner, L. C., Tarasov, L. & Tzedakis, P. C. An ice–climate oscillatory framework for Dansgaard–Oeschger cycles. *Nat. Rev. Earth Environ.* **1**, 677–693 (2020).
285. Kang, S. M., Frierson, D. M. & Held, I. M. The tropical response to extratropical thermal forcing in an idealized GCM: The importance of radiative feedbacks and convective parameterization. *J. Atmos. Sci.* **66**, 2812–2827 (2009).
286. Deplazes, G. et al. Links between tropical rainfall and North Atlantic climate during the last glacial period. *Nat. Geosci.* **6**, 213–217 (2013).
287. Peterson, L. C., Haug, G. H., Hughen, K. A. & Röhl, U. Rapid changes in the hydrologic cycle of the tropical Atlantic during the last glacial. *Science* **290**, 1947–1951 (2000).
288. Wang, X. et al. Interhemispheric anti-phasing of rainfall during the last glacial period. *Quat. Sci. Rev.* **25**, 3391–3403 (2006).
289. Ceppi, P., Hwang, Y. T., Liu, X., Frierson, D. M. & Hartmann, D. L. The relationship between the ITCZ and the Southern Hemispheric eddy-driven jet. *J. Geophys. Res. Atmos.* **118**, 5136–5146 (2013).
290. Chiang, J. C., Lee, S.-Y., Putnam, A. E. & Wang, X. South Pacific Split Jet, ITCZ shifts, and atmospheric North–South linkages during abrupt climate changes of the last glacial period. *Earth Planet. Sci. Lett.* **406**, 233–246 (2014).
291. Markle, B. R. et al. Global atmospheric teleconnections during Dansgaard–Oeschger events. *Nat. Geosci.* **10**, 36–40 (2017).

292. Buizert, C. et al. Abrupt ice-age shifts in southern westerly winds and Antarctic climate forced from the north. *Nature* **563**, 681–685 (2018).
293. Pedro, J. B. et al. The spatial extent and dynamics of the Antarctic Cold Reversal. *Nat. Geosci.* **9**, 51–55 (2016).
294. Rae, J. W. et al. CO_2 storage and release in the deep Southern Ocean on millennial to centennial timescales. *Nature* **562**, 569–573 (2018).

Acknowledgements
This work is supported by the National Key Research and Development Program of China (2018YFA0605700). X.Li is supported by the National Key Research and Development Program of China (2019YFC1509100), the National Natural Science Foundation of China (no. 41676190 and no. 41825012), and the Chinese Arctic and Antarctic Administration (CXPT2020015). G.A.M. was supported by the Regional and Global Model Analysis (RGMA) component of Earth and Environmental System Modeling in the Earth and Environmental Systems Sciences Division of the U.S. Department of Energy's Office of Biological and Environmental Research (BER) via National Science Foundation IA 1947282 and by the National Center for Atmospheric Research, which is a major facility sponsored by the National Science Foundation (NSF) under Cooperative Agreement no. 1852977. X.Y. is supported by the LDEO endowment for this work. M.R. is supported by the National Science Foundation, Office of Polar Programs (grant no. NSF-OPP-1745089). D.M.H. is supported by the Center for Global Sea Level Change (CSLC) of NYU Abu Dhabi Research Institute (G1204) in the UAE and NSF PLR-1739003. Q.D. is supported by Climate Variability & Predictability (NA18OAR4310424) as part of NOAA's Climate Program Office. R.L.F. was supported by the National Science Foundation under grant no. U.S. NSF PLR-1744998. B.R.M. was supported, in part, by a Stanback Postdoctoral Fellowship. D.H.B. was supported by the U.S. NSF award OPP-1823135. S.P.X. was supported by the National Science Foundation (AGS-2105654, AGS-1934392 and AGS-1637450). S.T.G. was supported by the U.S. NSF awards PLR-1425989 and OPP-1936222, and by the U.S. Department of Energy (DOE) (award DE-SC0020073). M.A.L. is supported by the Office of Polar Programs, National Science Foundation grant (no. 1924730). X.Chen is supported by the National Key Research and Development Program of China (2019YFC1509100) and the National Science Foundation of China (no. 41825012). S.E.S. was supported by the National Science Foundation under grant no. U.S. NSF PLR-1440435. M.M.H. was supported by the National Science Foundation under grant no. U.S. NSF OPP-1724748. S.F.P. is supported by the U.S. Department of Energy Office of Science, Biological and Environmental Research programme. Z.W. is supported by China National Natural Science Foundation (NSFC) project nos. 41941007 and 41876220. E.P.G. is supported by the NSF grant AGS-1852727. H.G. is a research director within the Fonds de la Recherche Scientifique-FNRS. C.Y. is supported by the National Research Foundation of Korea (NRF) (grant NRF-2019R1C1C1003161).

Author contributions
X.Li, W.C., G.A.M., D.C., X.Y., M.R., D.M.H., Q.D., R.L.F., B.R.M., G.W., S.F.P., C.X., B.W., X.Chen and P.R.H. wrote specific sections or subsections, and provided figures for the Review. All authors contributed to the manuscript preparation, interpretation, discussion and writing.

Competing interests
The authors declare no competing interests.

Peer review information
Nature Reviews Earth & Environment thanks the anonymous reviewers for their contribution to the peer review of this work.